2008

Wireless mote-based in-process diagnostics using hand-held tools in network enabled manufacturing environments

Reghu Anguswamy

Department:

WIRELESS MOTE –BASED IN-PROCESS DIAGNOSTICS USING HAND-HELD TOOLS IN NETWORK ENABLED MANUFACTURING ENVIRONMENTS

by

REGHU ANGUSWAMY

A THESIS

Presented to the Faculty of the Graduate School of the

MISSOURI UNIVERSITY OF SCIENCE AND TECHNOLOGY

In Partial Fulfillment of the Requirements for the Degree

MASTER OF SCIENCE IN SYSTEMS ENGINEERING

2008

Approved by

Jagannathan Sarangapani, Advisor

Can Saygin, co-advisor

Cihan H. Dagli

PUBLICATION THESIS OPTION

This thesis consists of the following two articles that have been submitted for publication as follows:

Pages 5-35 appear in the INTERNATIONAL JOURNAL OF MANUFACTURING RESEARCH

Pages 36-72 are intended for submission to the INTERNATIONAL JOURNAL OF DISTRIBUTED SENSOR NETWORKS

ABSTRACT

When complex manufacturing systems are considered, post process inspection can be a very time consuming and costly. In addition, no inspection data is typically collected unless a major problem is encountered. Real-time monitoring of the manufacturing processes and verification of its product quality are two important factors to reduce the manufacturing lead time and to ensure safety and quality.

In this thesis, a diagnostics and root-cause analysis scheme with a single channel wireless routing protocol for real-time monitoring of process quality of pull-type fastening operations is first presented. The overall architecture has been implemented on a Huck45 pull-type tool, which is a hand-held pneumatic fastening tool used extensively in the aerospace industry, with lock-bolt fasteners. The proposed architecture (1) detects quality problems in real-time during the fastening process and (2) reduces post-process inspection. Extensive hardware results by using the hand-held tool are included.

On the other hand, due to tool mobility, ad-hoc wireless networking routing protocol is necessary to enable real-time monitoring and increase the process visibility. Thus, in the second chapter of this thesis, a novel multi-channel energy efficient routing protocol for ad hoc wireless networks that ensures network quality of service (QoS) in terms of throughput and end-to-end delay is introduced for such hand-held tools. The network QoS effects the overall monitoring when multiple tools are utilized. The performance of the multi-channel multi-interface routing protocol for network-enabled manufacturing environments was successfully verified using Ns2 simulations and contrasted with a single channel routing protocol implemented in Chapter 1 of the thesis.

ACKNOWLEDGMENTS

I am extremely grateful to my advisors, Dr. Sarangapani and Dr. Saygin, for the encouragement and guidance they have given me and the extreme patience they have shown in my completing this work. They have also given me sufficient freedom to explore avenues of research while correcting my course and guiding me at all times. I thank Dr. Dagli, my committee member and Department Chair, for the help and financial support he has provided during part of my Masters' degree program and rest by Air Force Research Laboratory (AFRL). This study was funded by the AFRL under the contract FA8650-04-C-704 through the Center for Aerospace Manufacturing Technologies (CAMT) at the University of Missouri-Rolla (UMR) and NSF I/UCRC Center for Intelligent Maintenance Systems (IMS).

I thank Dr. Maciej Zawodniok, Jeff Birt, Dr. James Fonda, Anil Ramachandran and Ahmet Soylemezoglu, without whose help, this effort and its successful completion would not have been possible. Special thanks go to all members of the IMS and AutoID/ESNL research groups who have stood by me at all times.

On a personal note, I thank my parents P Anguswamy and A Annakkodi, for the tremendous encouragement and support I have received throughout my life which has enabled me to face the challenges and achieve success.

TABLE OF CONTENTS

LIST OF ILLUSTRATIONS

INTRODUCTION

PAPER I

PAPER II

LIST OF TABLES

PAPER I

PAPER II

1. INTRODUCTION

Manufacturing environments in the aerospace industry are becoming more efficient by incorporating and integrating the rapid development of new technologies in areas such as electronics, communications, computing etc. This has also led to process monitoring and quality assurance of products gaining significant importance in the world of manufacturing. Maintenance through improved diagnostics and prognostics with on board computing are fast gaining significance in the shop-floor environments improving the cost efficiency and reducing the maintenance downtime. Overall, they also play a significant role in ensuring the quality of the processes and products.

1.1 Network-Enabled Manufacturing

Tools in modern day manufacturing shop floors are being equipped with on board computing capability and network connectivity. Such networks enabled environment (Figure 1.) makes the engineers more efficient and effective in monitoring and scheduling the processes. The personnel would be able to monitor for failures and monitor performance remotely by analyzing the data from the network. Network-enabled environment also provides a platform for diagnostics in real-time at both component and the system levels. In such aerospace manufacturing environments, hand held tools are widely utilized for operations such as fastening. Unfortunately, fastening being labor intensive operation, problems arise causing degraded product quality costing the airline industry significantly due to end inspection. Additionally, end inspection of such fastening operations is not only expensive but also causes delays.

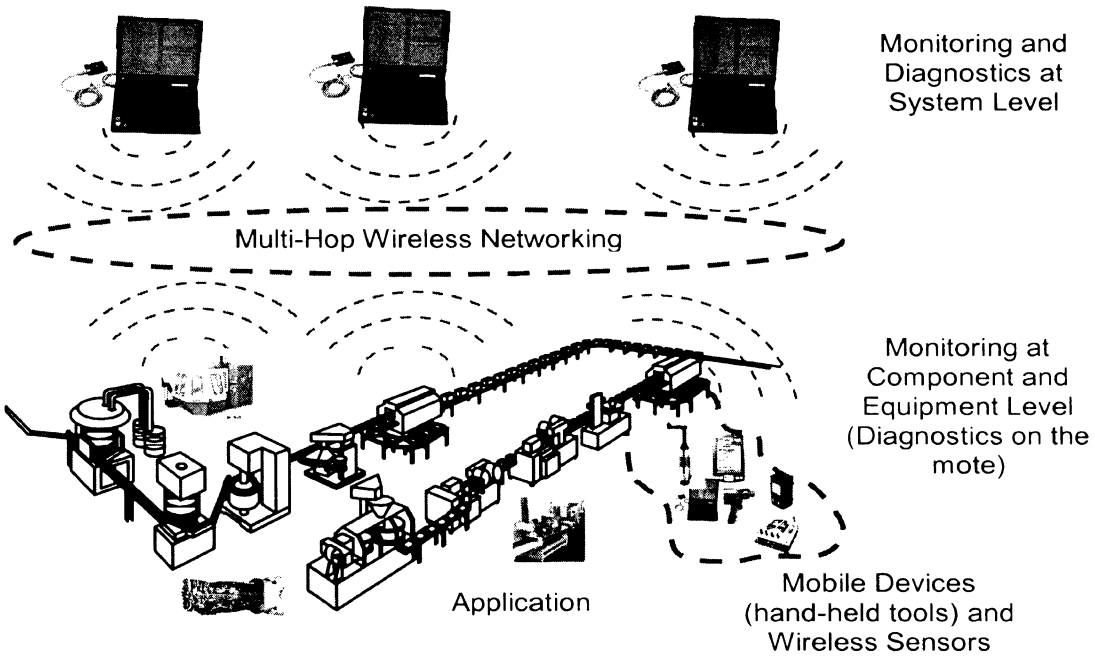

Figure 1: A network enabled manufacturing environment

Therefore two major issues have been addressed in this thesis for network-enabled manufacturing shop floor systems using hand-held tools:

1. Incorporating intelligent behavior– hand-held tools equipped with embedded sensors and on-board processing/computing capabilities making them possible the in-process diagnostics of tool operations and products in real-time; also, wireless capability for the tools add significant advantages to the network-enabled environment:
    a. Wireless capability of the tools increases the mobility of the tools in the shop floor which may not be the case if they are wired. Wireless ensures safety
    b. the hand-held tools become more complex and cumbersome to use if additional wires are added to the tool

2. Data management – a typical shop floor environment will have many tools operating simultaneously forming an ad hoc wireless networks and the network requires efficient protocols such as routing and scheduling for handling the voluminous data generated. Although decisions have to be made on the tool, the data still need to be stored in a central repository for detailed analysis.

1.2 Outline of the Thesis

The thesis has been presented in the form of two papers. The first paper deals with the in-process monitoring of the product quality in terms of the fastener grip length for hand-held pull-type fastening tools. The pull type tools are equipped with embedded sensors and a novel diagnostic methodology to detect the fastener grip length in real-time using the data generated from the sensors. The diagnostic methodology was successfully implemented on the tool delivered by Boeing using on-board computing capability to verify the fastener grip length in real-time. Wireless communications was also enabled on the tool for remote monitoring and maintaining the mobility of the tool.

Currently, the fastener grip lengths for pull-type tools are verified during post-process by special personnel through manual inspection using calibrated gages. On board diagnostics with remote wireless monitoring removes the need for manual inspection thereby reducing the labor costs and ensuring the quality of the product. In the manufacturing of an aircraft, as many as a million fasteners may be used. Thus, such real-time monitoring also saves cost by identifying the wrong fastener grip lengths being used than in the case of manual inspection. In this chapter, an existing single channel routing protocol referred to as OEDSR: Optimal Energy-Delay Subnet Routing will be utilized.

The second paper proposes a new routing protocol for multi-channel ad hoc wireless networks. In such manufacturing shop-floor environments involving high number of such hand-held tools generates large quantities of data requiring the data to be transmitted in a multi-channel based wireless networks. Compared to single channel wireless networks, multiple non-interfering channels, if used, would improve the amount of data traffic that can be handled in the network lowering congestion and dropped packets while maintaining end-to-end delay and energy efficiency. The new protocol considers data throughput maximization, energy efficiency and minimizing end to end delay for data.

PAPER I

IN PROCESS DETECTION OF FASTENER GRIP LENGTH USING EMBEDDED MOBILE WIRELESS SENSOR NETWORK-BASED PULL TYPE TOOLS

Reghu Anguswamy
Engineering Management and Systems Engineering
Missouri University of Science and Technology – Rolla, Missouri, U.S.A 65401
Email: radk7@mst.edu

Can Saygin
Mechanical Engineering
University of Texas, San Antonio – San Antonio, Texas, U.S.A 78249
Email: can.saygin@utsa.edu

S. Jagannathan
Electrical and Computer Engineering
Missouri University of Science and Technology – Rolla, Missouri, U.S.A 65401
Email: sarangap@mst.edu

ABSTRACT

In this paper, a diagnostics and root-cause analysis scheme for real-time monitoring of process quality of pull-type fastening operations is presented. The proposed approach encompasses (1) integrating a strain gage, an LVDT (Linear Variable Differential Transducer), a pressure sensor, and a mote on a pull-type pneumatic tool; (2) monitoring process parameters coming from embedded sensors communicated wirelessly via the mote and generating process signatures in real-time; and (3) detecting anomalies in real-time in the process signatures for quality problems related to the grip length deviation in pull-type fastening operations. A feature extraction-based diagnostic methodology is employed to make decisions in terms of grip length deviations in the form of normal grip, over grip, and under grip. The process signature of strain-over-displacement versus displacement has shown unique features that are extracted to

determine the quality of the fastening process. In addition, air pressure is also continuously monitored in real-time during the process since it also affects the quality of the fastening operation.

The overall architecture has been implemented on a Huck45 pull-type tool, which is a hand-held pneumatic fastening tool used extensively in the aerospace industry, with lock-bolt fasteners. The prototype has been tested under a variety of experimental settings in order to verify its effectiveness and validate its performance over a wide range of different sheet metal thicknesses used for fastening. The experiments have shown that the proposed approach is successful, with an accuracy of over 96%, in determining the quality of fastening operations and in communicating the quality information in real-time using a wireless network to a server. Overall, the proposed architecture has merits to (1) detect quality problems in real-time during the fastening process and (2) reduce post-process inspection, thereby improving quality while reducing cost. In addition, the proposed approach facilitates 100% data collection on each fastener as opposed to traditional statistical process control (SPC) techniques, which rely on sampling.

Keywords

Automatic inspection, fasteners, automation, communication systems, wireless networks

1. INTRODUCTION

Hand-held fastening tools are extensively used in manufacturing, especially in aerospace industry. Such tools are prone to human error; typically the process is monitored by the operator and joints are visually inspected with very limited use of gages after the process is completed. Installation of fasteners may incur up to 80% of the total fastening costs while the remaining 20% is for procurement of fasteners [1]. When

complex products, such as an aircraft, are considered, fastening process and its inspection can be a very time consuming task. In addition, no inspection data is typically collected during the process unless a major problem is encountered. Real-time monitoring of the fastening process and verification of joint quality are two important factors to reduce the manufacturing lead time while ensuring safety and quality.

In this study, a pull-type fastening tool has been (1) integrated with sensors and (2) equipped with a mote for on-the-tool, real-time decision-making and wireless communication. The tool is capable of monitoring pull-type fastening processes and determining the grip length deviation for joints as normal grip, under grip, or over grip employing the decision-making methodology that resides on the mote.

As shown in Figure 1, a typical pull-type (i.e., tension) tool operates as follows:

1. Fastener is inserted into the hole and the collar is placed over the fastener pintail.
2. The tool nosepiece is placed on the shank of the fastener. When the tool is actuated, the pintail is pulled against the push on the collar. As a result, the head of the fastener is seated into the hole and the tool starts swaging the collar.
3. Continued swaging of the collar forces the collar material into the pin locking grooves creating an extrusion action that stretches the collar, which results in a corresponding stretch of the pintail.
4. When collar is completely swaged (i.e., collar is resting against the plate), the tool continues pulling the pintail until it breaks at the break neck groove. The nosepiece is then removed away form the joint and the pintail is discharged.

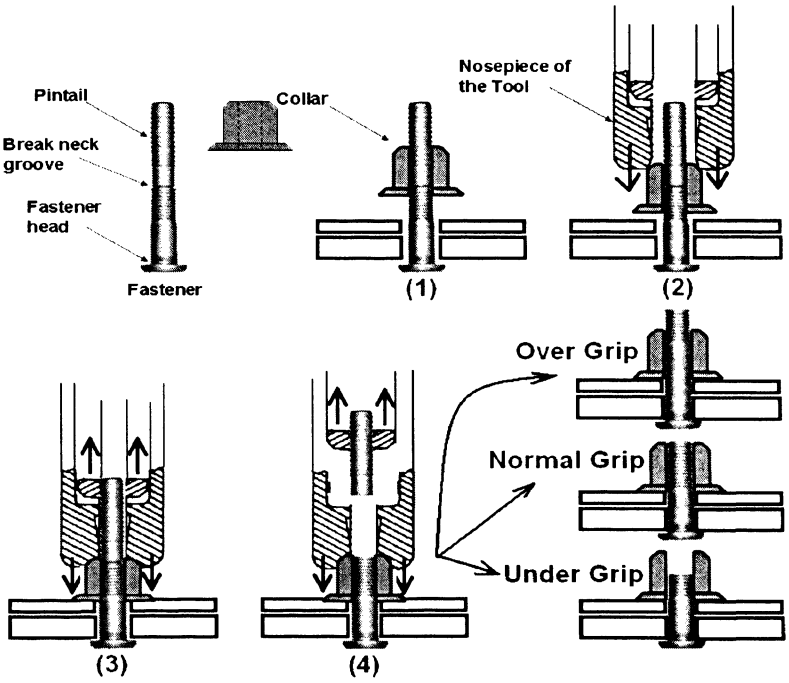

Fig 1: Operation of the Fastening Tool and Types of Grip Length Deviations

One of the quality issues for this operation is caused by a mismatch between the fastener/collar length and the plate thickness. If the plates are thicker or equivalently the fastener is shorter, then the break neck grove stays inside the collar, which is the under-grip condition. If the plates are thinner or equivalently the fastener is longer, then the break neck grove sticks out of the collar, which is the over-grip condition. In both cases, the strength of the joint is compromised. As shown in Figure 1, for normal grip condition, the sizes of the plates and the fasteners match so that the break neck groove breaks almost flush with the top of the collar.

The focus of this study is to automatically determine the grip length deviation as normal grip, under grip, or over grip in real-time during the operation of a sensor-

integrated tool and to communicate this information to a centralized database server via wireless networking.

2. LITERATURE SURVEY

The most common approach to ensure that fasteners of correct grip length are being used in a fastening operation is to use gages and probes after the operation is completed. Such post-process inspection techniques increase the overall manufacturing lead time since they are conducted as a stand-alone process using a different tool than the fastening tool. Due to this fact, joints are usually inspected on a sampling basis, as opposed 100% inspection. Therefore, not only the manufacturing lead time is increased but also some defective joints can pass through unnoticed.

A survey of patents in this area is summarized in Table 1. The techniques are either pre-process or in-process monitoring. In pre-process monitoring the fastener grip length to be used are detected using measuring probes [2, 3], image processing systems [4] or measuring gages [5, 6]. In-process monitoring address detection methodologies for quality issues and failure modes such as proper orientation of fasteners [7], improper fastener head heights [8], improper rivet lengths [9], improper fastening joints due to insufficient force deformation [10] and improper plate thickness [11, 12]. In [11], the authors propose a methodology for detecting under grip and over grip cases and improper material usage using a clamping analysis, which is based on pressure (of hydraulic fluid acting on the rivet mandrel) and displacement (of the air piston) signatures. Since such fastening tools are very compact in design, it is very difficult to retrofit them with sensors installed inside the tool. In addition, the proposed methodology for under grip and over grip detection is purely based on displacement signature and hence may be unreliable.

Table 1. Summary of Patents

Reference	Patent Number	Title	Author(s)	Year	Scope	Quality Problems
[2]	4,649,753	Verification probe	D. Goodsmith	1987	Pre-process verification probe for selecting the proper grip length for fastener installation	Improper fastener length
[3]	4,876,800	Portable grip length indicator	G. Pekar J. Mason M. Blane	1989	Pre-process fastener grip length measuring technique using a portable probe for selecting the proper grip length for fastener installation	Improper fastener length
[4]	5,727,300	Fastener verification system	M. Ekdahi J. Hanks B. Hiller J. LaChapelle K. Thomas M. Turley	1998	Automatic fastener selection prior to installation: Image based - determines the fastener size to be installed and then has an automation to get the right fastener to be installed	Selection of right fastener prior to installation
[5]	7,065,897	Fastener Grip Length Selector	J. Luner L. Hoeckelman	2006	A measuring gage to determine the grip length of fastener required when a temporary fastener is installed in a hole on the assembly	Pre-process detection for selecting the right length fastener
[6]	7,070,375	Fastener Grip Length Indicator	L. Hoeckelman	2006	Grip length determination technique using a mechanical measuring gage	Pre-process detection for selecting the right length fastener
[7]	4,237,612	Fastener grip length measuring system	E. Christian R. Blunck	1980	In-process fastener grip length measuring technique based on a hand held measuring device utilizing an insertable sliding probe	Improper material or structural part thickness
[8]	5,673,839	Real-time fastener measurement system	B. Howard J. Avery	1997	Measurement of fastener head heights in real-time using 3 embedded proximity sensors – for flush head fastener types	Improper fastener head heights

[9]	6,276,050	Riveting system and process for forming a riveted joint	D. Mauer H. Roeser R. Opper A. Wojcik C. Schoenig	2001	Sensors and an electronic control unit to determine the riveting/actuator characteristics using force vs. distance signatures	Improper riveting/actuator characteristics (incorrect rivet length and actuator power output)

Wireless monitoring for such pneumatic tools is available in the literature [13] where the pressure is continuously monitored and sends out a radio frequency (RF) signal to the base station when the pressure reached a pres set value. When the base station receives an RF signal, it records a successful operation. As long as the base station does not receive any RF signal, the tool is not working satisfactorily. Thus, it does not present any on-board/on-tool processing and decision making for the operator to have first hand knowledge of the process quality.

Several other studies are available in the literature for in-process monitoring and detection of failures in fastening operations, such as the Newton-Raphson Method for threaded fasteners to detect improper fastener alignment [14,15], statistical pattern recognition in thermal system protection panels to monitor the structural health of fasteners being installed [16], least square method based on Torque versus Insertion Depth curves for screw insertions [15, 17] to detect improper fastener alignment, and the weightless neural network based monitoring of screw fastenings in automated assembly to detect improper fastening operations due to screw jamming, screw wedging, thread stripping or cross threading [18].

The approach proposed in this paper is unique due to the following reasons:

1. It is based on extracting unique features from process signatures generated in real-time with data obtained from strain and displacement sensors; such an approach has not been investigated previously.
2. The sensors are installed on the exterior of the tool; thus no redesign of the tool is necessary.
3. The prototype fastening tool is equipped with not only process-related sensors, such as strain, displacement, and pressure sensors, but also with real-time, on-the-tool decision making and wireless communication capabilities to communicate the result to a base-station [19]. It is extremely important to have wireless communication to facilitate tool and operator mobility and safety concerns due to wiring.
4. By combining the fastening feature with inspection capability on a single tool, the proposed approach allows for data collection on 100% of the joints in real-time as opposed to sampling-based statistical process control methods that are applied post-process as stand-alone operations, which increase the manufacturing lead time.

3. PULL TYPE FASTENERS AND TOOLS: THE UNDERLYING CONCEPT

As shown in Figure 1, the pintail breaks off at the end of the process and the remaining portion of the fastener with the collar form a permanent joint. The underlying concept is very similar to a tensile test in terms of stress-strain relationship. During the fastening process, the outer sleeve of the nosepiece rests against the collar causing it to swage, while the inside jaws pull the pintail. The pintail goes through its yield point, passes from the elastic range to the plastic range, then reaches its ultimate tensile

strength, and finally at its fracture point it breaks and the process is completed. While the pintail of the fastener is going through this sequence, the outer sleeve of the nosepiece stays under compression pushing the collar against the plates. Due to superior material properties of the nosepiece compared with the materials properties of the fastener, the outer sleeve of the nosepiece goes through a slight elastic deformation (i.e., no plastic deformation occurs on the nosepiece) during the process and when the process is completed, it recovers back to its original state.

The preliminary studies that led to the approach proposed in this study have shown that there is a relationship between the elastic deformation occurring on the nosepiece and the elastic-plastic deformation on the fastener. In order to use this relationship, the nosepiece of the tool has been integrated with a strain gage that shows the elastic deformation, in the form of compression, of the nosepiece. This behavior has been plotted as Strain versus Time to generate a process signature. In order to investigate the impact of grip length on the strain-time process signature, different combinations of plates have been tested. In addition, plates with rubber washers in between have also been tested to investigate the impact of material properties on the process signature.

As shown in Figure 2, the test results have shown visible differences among process signatures. Therefore, for a given combination of plates and fasteners, there is a unique process signature. Any deviation from this unique signature is a sign of abnormality, which could be a quality problem. The reliability of this approach depends on how much variability in the process signature can be attributed to noise, such as the way the operator holds the tool, and how much variability is caused by the mismatch between the plate thickness and the fastener length.

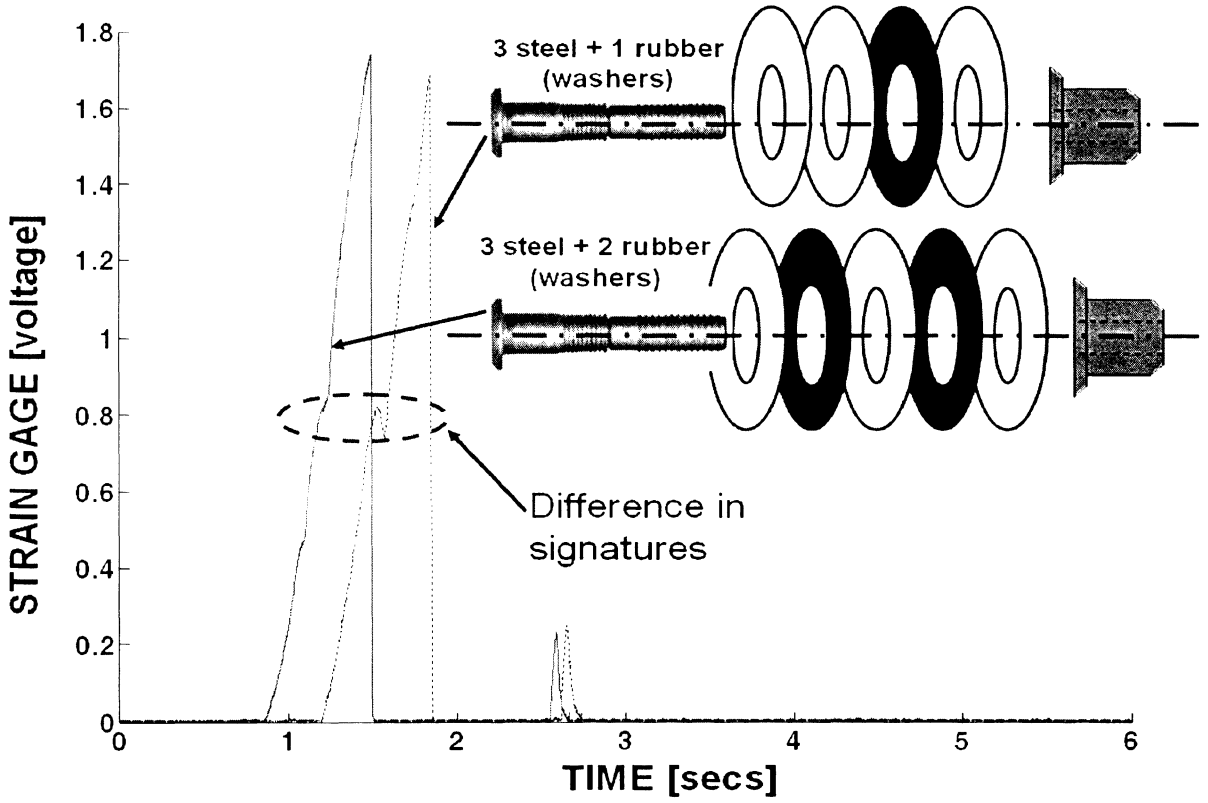

Fig 2: Process Signatures

Fastening processes are required to yield a certain amount of clamping force, which is the force acting on the joined members after the operation is completed [1]. Swaging of the collar onto a certain number of grooves on the fastener's shank ensures a certain level of clamping force. If the collar is not in contact with the right number of grooves, then the fastening operation will not yield the desired level of clamping force. The total thickness of the joined members with respect to the length of the fastener affects the number of grooves to come in contact with the collar. For both over grip and under grip cases, there are fewer grooves in contact with the collar; thus clamping force on the joint is less than the design requirement.

Ensuring right grip length is extremely costly for manufacturing environments where a particular product is made up of different thicknesses of materials and requires many different types and sizes of fasteners. Aerospace industry is a good example that falls under this category. In such aerospace assembly plants, fasteners of different grip lengths may be chosen using different techniques, such as a fastener grip length selector/gage [2-6]. Nevertheless, such selections made prior to production do not guarantee that there will not be a mismatch between the plates and the fasteners. The proposed approach provides a solution to detect such a mismatch at the point of use.

4. REAL TIME DETECTION OF GRIP LENGTH DEVIATION: THE PROPOSED APPROACH

As shown in Figure 3, three sensors have been integrated with a pull-type fastening tool in order to implement the proposed data collection scheme. A resistive-type strain gage is placed on the nosepiece of the tool and used in a quarter bridge configuration with a nominal resistance of 120 Ω. During fastening operation, the strain gage measures the strain on the nosepiece by developing a differential voltage output due to change in resistance.

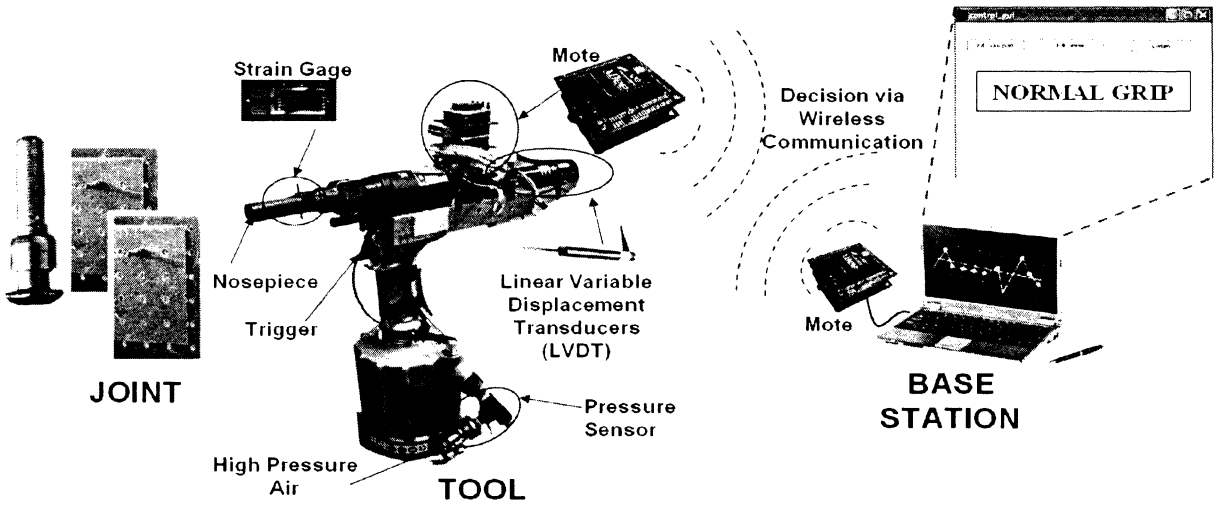

Fig 3: Sensor-integrated Pull-type Tool with Wireless Communication Capabilities

A linear variable differential transformer (LVDT) with a sensitivity of 181.4 millivolts/mm is integrated in order to measure the displacement of the inner jaws in the nosepiece during the fastening operation. Finally, a pressure sensor with a sensitivity of 29.5 millivolts/psi is attached at the air inlet port of the tool in order to measure pressure variations in process. At low pressures, which can happen in industrial settings when there are several pneumatic equipments and tools operating at the same time, the tool sends a low pressure signal to the server without executing the proposed grip length detection methodology.

The nosepiece strain data from the strain gage conditioning layer are calibrated through simulation of known strain values by connecting the respective values of calibration resistors R_{cal} as calculated by the equations below:

$$\Delta R = \varepsilon_{sim} \cdot GF \cdot R_g \tag{1}$$

$$\Delta R = R_g - \frac{R_g \cdot R_{cal}}{R_g + R_{cal}} \quad (2)$$

$$R_{cal} = \frac{\Delta R \cdot R_g}{R_g - \Delta R} \quad (3)$$

where

ε_{sim} : Simulated strain,

GF : Gage factor set to 2.07, and

R_g : Nominal resistance of strain gage (120Ω).

Thus, resistors of 36kΩ, 100kΩ, and 240kΩ corresponding to strain values of 1,604 microunits, 580 microunits, and 240 microunits, respectively, are connected in parallel to the R_g. The corresponding differential voltages are then measured and plotted as strain versus output voltage to obtain a slope S. The strain is then calibrated from the output voltage as follows:

$$\varepsilon = Vo \times S \quad (4)$$

where

Vo : Output voltage

S : Slope on strain versus voltage plot

ε : Strain developed

The sensor data are processed on the mote and the decision (i.e., normal grip, under grip, or over grip) is communicated to the centralized database server over a wireless sensors network. The 5-layer stack mote includes the following layers:

1. Power layer: This layer supplies regulated power supply of ±5V to the sensors and 3.3V to the processing layer and the communication layer. The power layer accepts a bipolar input in the range ±7.2V to ±10V.

2. Sensor input layer: Output voltages from the sensors are fed to the processing layer through this layer.
3. Strain gage conditioning layer: Strain gage conditioning is done on this board. The strain gage placed on the nosepiece is operated in a quarter bridge configuration. Two potentiometers on this board allow setting the offset and the gain of the out voltage.
4. Processing layer: This layer is built based on a Silabs® C8051F120 processor for processing the sensor data and provide the decision to the communication layer.
5. Communication layer: This layer is built based on a MaxStream® XBee wireless radio communication, sends the decision received from the processing layer to the server.

4.1 Process Signature Analysis: Initial Testing

Initial experiments have shown that there are unique features in Strain-Time and Displacement-Time signatures that can be used to differentiate grip lengths, as shown in Figure 4. On the other hand, due to variations within each grip length category, these signatures alone are not robust enough to detect normal, over, and under grip conditions with high confidence.

In order to amplify the effect of grip length deviations on process signatures, a new parameter, namely Strain/Displacement ratio (S/D), has been introduced. By using the primary sensor data (i.e., nosepiece strain and displacement), a compound process signature Strain/Displacement versus Displacement has been developed. As shown in Figure 5, normal grip data exhibits a unique bowl-shaped dip. In addition, over grip and

under grip data are also unique. Therefore, presence of a bowl-shaped dip points to a normal grip case.

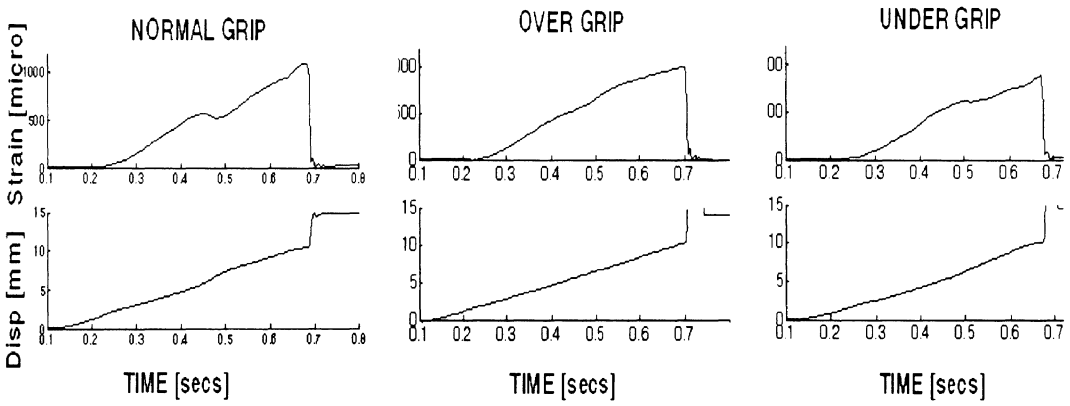

Fig 4: Process Signatures for Different Grip Length Deviations

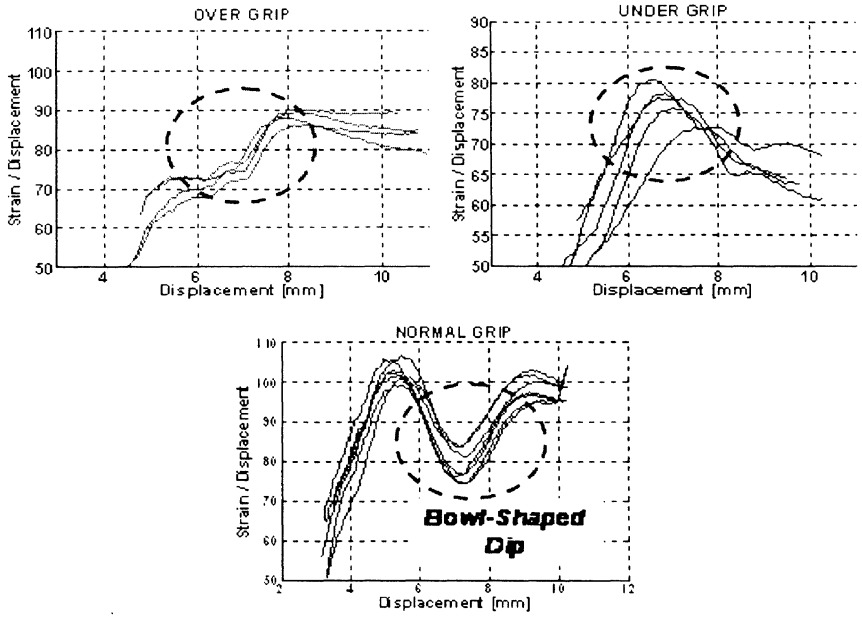

Fig 5: Strain/Displacement versus Displacement Signatures: Visible Differences

4.2 Real-time Feature Extraction and Decision-Making

In real-time, the strain and displacement data are continuously monitored in time. The data are collected at 5,000 samples per second and smoothened by averaging every 20 samples. Each smoothened strain and displacement data are calibrated and S/D is calculated.

There are three unique features that are used to detect grip length variations. First one is the peak strain on the strain-time signature, which occurs right before the tool completes the fastening operation. The other two features are on the strain/displacement-displacement signature; depth and half-width (will be referred to as width for the rest of the paper) of the bowl measured.

As shown in Figure 6, the fastening operation starts at t_{start}, which is the time at which the strain value exceeds 80 microstrain. Based on the observations during the initial experimentation, the fastening operation is completed when the strain value drops by at least 100 microstrain than its previous value, which is shown as t_{end}. The peak strain (ε_p) is extracted as the strain value at time tend. As sensor data are received, S/D is calculated in real-time period from t_{start} to t_{end}. It has been observed that the first max (f_1) is detected when at least 4 recent, consecutive S/D values are lower than the previous 4 S/D values, which occurs at time t_0. The first min (f_2) is detected as the minimum value of S/D between t_0 and t_{end} , which is time t_1. Therefore, width (on the displacement-time signature) is calculated as $W = d_1 - d_2$, and depth (on the S/D-time signature) is calculated as $D = f_1 - f_2$.

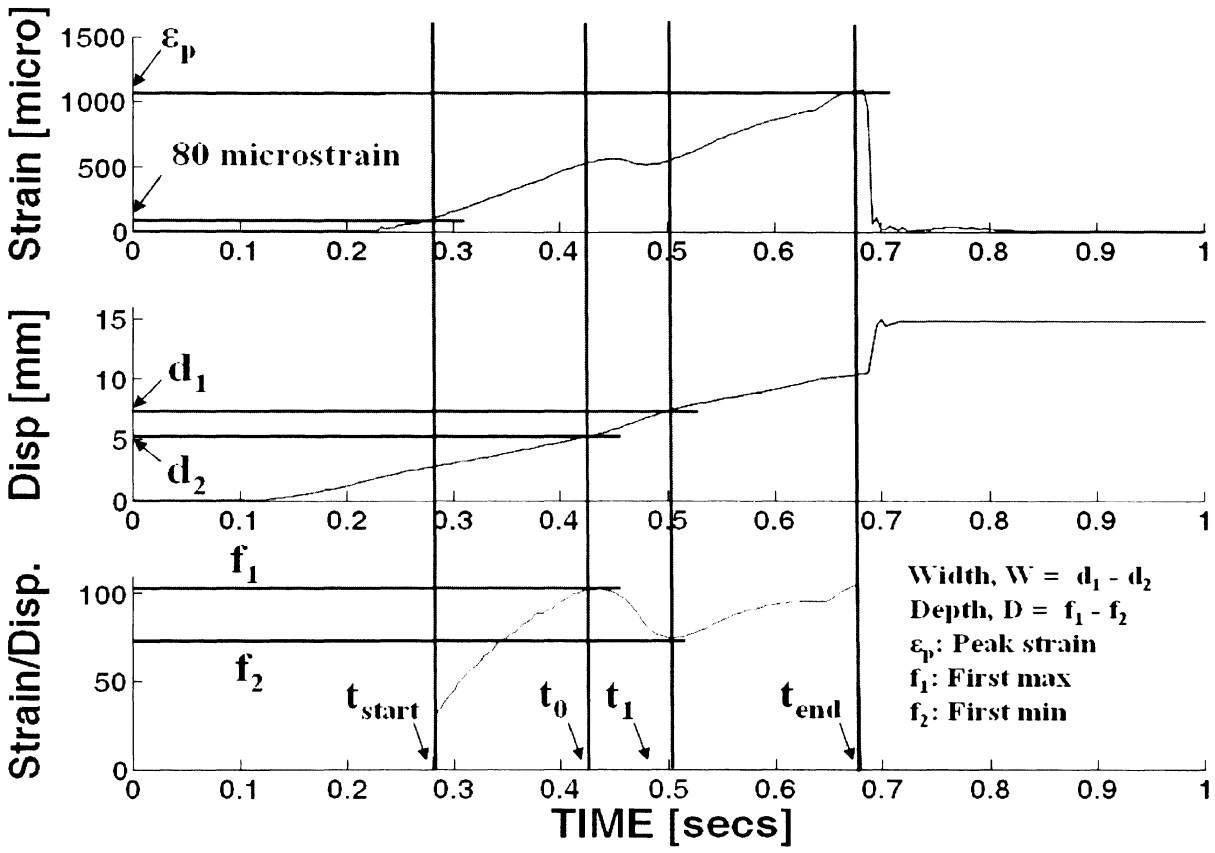

Fig 6: Real-Time Feature Extraction

These extracted features are then used for decision-making. If the depth, D, of the dip is greater than the limit set for the depth for normal grip and width of the dip is less than the limit set for the width for normal grip, then the decision is made as normal grip. Otherwise, it is improper grip, which is either over grip or under grip. If the peak strain is less than the under grip limit, then the decision is made as under grip, else it is over grip. The real-time decision making process is depicted in Figure 7.

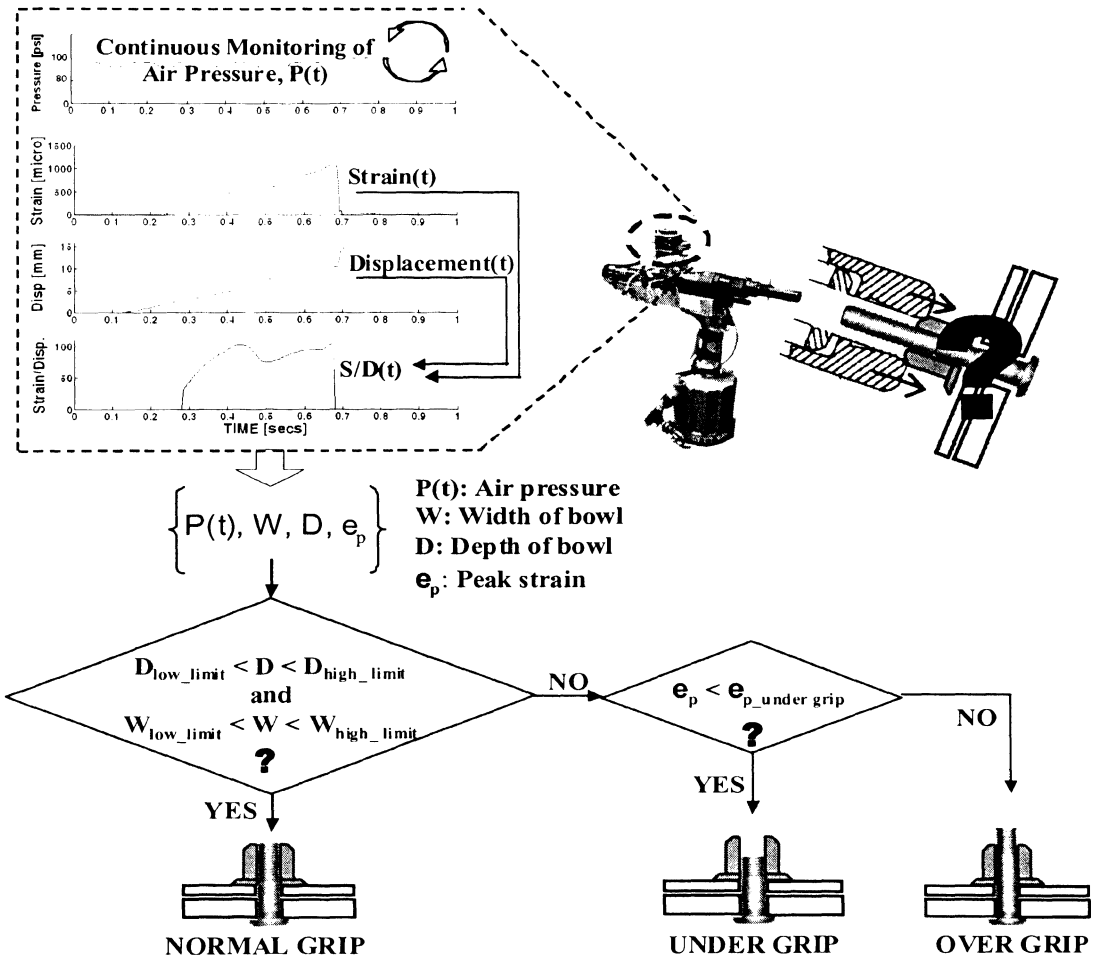

Fig 7: Real-Time Decision Making Process

4.3 Variability and Setting Limits

In order to implement the decision-making process outlined in Figure 7 and to properly detect the type of grip, variation in depth (D), width (W), peak strain (ε_p), and pressure have been studied based on 15 samples (i.e., data from 15 fasteners). The 15-sample data set has been used as training data to set the limits in order to implement the decision-making process, which is followed by testing of the tool to validate the performance of the proposed approach. The implementation phase is described in Sections 5 and 6.

As shown in Figure 8, the limits for depth of bowl-shaped dip for normal data are 5 mm and 25 mm. Similarly, the limit for width is 0.25 mm and 2 mm. In order to differentiate over grip from under grip, peak strain for under grip is used, which has limit of 930 microstrain.

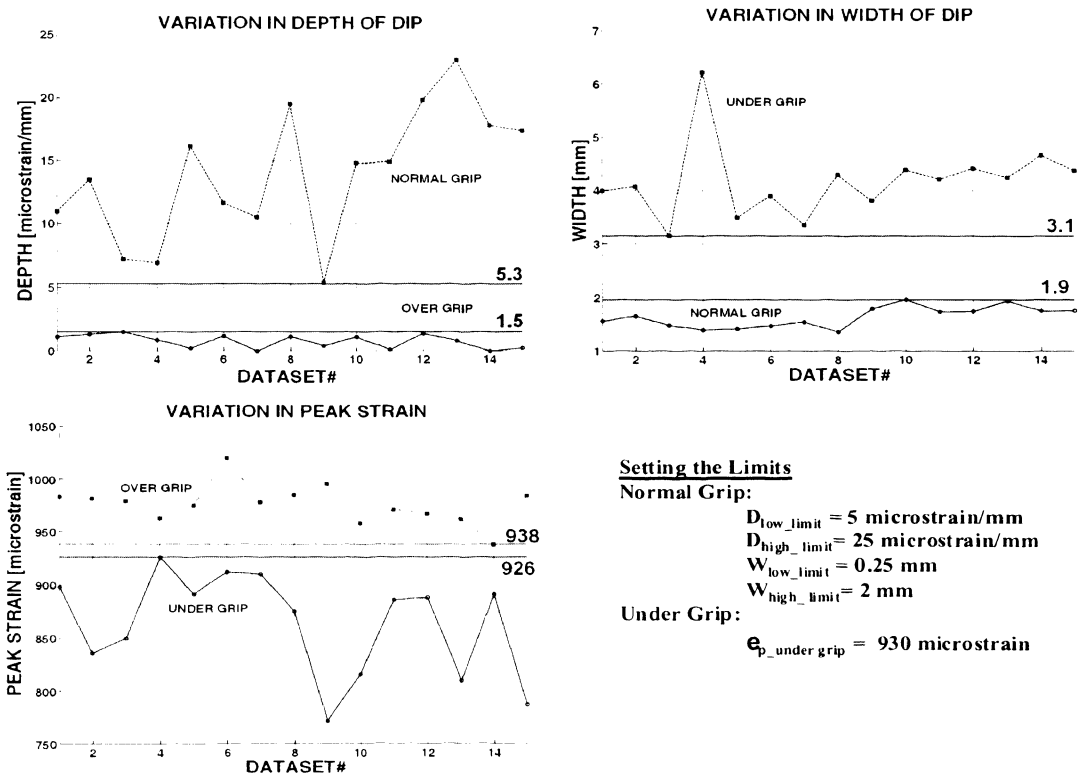

Fig 8: Variability in Sample Data

The fastening tool used for prototype development and experimentation requires a minimum of 85-90 psi of inlet air pressure for proper operation. If the pressure drops below 85 psi during the operation, the decision making process is not executed; instead a low pressure message is sent from the mote to the base station. The joint is considered potentially defective.

In general, several factors can contribute to variability in data: tolerance on plate thickness, sensitivity of sensors on the tool, and operator. The manufacturers specify a tolerance range for plates. For instance, a plate of a nominal thickness of 7.4mm has been used during experimentation for under grip cases. According to the specifications sheet, the tolerance on the plate is ± 0.4mm. Hence, the variability in plate

thickness could vary from 7.8mm to 7mm. Since this paper present a prototype tool, rather than a production-ready tool, no measurements were made on plate thickness at the joints during validation of the proposed proof-of-concept model. Therefore, tolerance on plates is introduced here as a factor that can cause potential variation in data in actual production environments, not necessarily as a factor that has caused variations in the experiments presented in this study.

Another factor is the sensitivity of the sensors integrated with the tool. For instance, the strain gage used on the nosepiece has a 120 ohm configuration with ± 0.0015 % variability in resistance. It yields a variability of ± 7.24 microstrain. Similarly, the displacement data are acquired via an LVDT, which has a sensitivity of ± 6.2 nanometer per mm. Consider the following example. For 500 microstrain and 5 mm displacement, the nominal value for S/D is 100 microstrain/mm. When the variation is considered, it is possible that this value could range from 98.56 to 101.44. The training data set (15 samples) has been studied to ensure that the limits set for the decision-making model are farther apart than the potential variability that can be introduced due to the sensitivity of the sensors.

Operator variability can also play a major role in variation in an actual production environment. During the development phase of this study, several trips were made to industry to observe how the tool is actually being used. It was observed that, for instance, some operators would operate the tool by holding it at a different angle than the other operators. Similarly, using both hands or pressing harder on the nosepiece by using the body weight is a common practice. In order to avoid the potential effect of operator

variability, only one person has collected data during the experimentation phase of this study.

Another factor that has been considered in this study is material properties. In order to investigate the impact of material properties, aluminum (Modulus of Elasticity, E = 74 GPa) and copper (Modulus of Elasticity, E = 130 GPa) plates of same thickness have been tested. In terms of depth, width, and peak strain, the analysis of the data obtained form both plates has shown no statistical significant difference between the two plates. Therefore, the proposed methodology is insensitive to changes in material properties, specifically for the modulus of elasticity in the range of 70-130 GPa. However, when a 4-mm thick rubber washer is placed between two plates with a total thickness that falls in the normal grip range, the process signatures are extremely different than what has been observed without the rubber washer.

5. WIRELESS SENSOR NETWORKING

Wireless sensor network (WSN) with embedded mobile hardware developed at the University of Missouri – Rolla (UMR) have been used to deploy sensing capability, diagnostic methodology, and efficient communications. As indicated earlier, wireless networking is the key for the operation of the tool since it allows tool and operator mobility. Wired networking is avoided because of safety concerns. Due to tool mobility in the shop floor environments where the fastening operations are performed, traditional one hop communication may not be the option of choice. Instead, a truly multi hop non-line of sight communication protocol, which is energy efficient, is necessary for decision and data transfer between the tools and the central database.

5.1 Architecture

The tool is integrated with embedded mobile hardware (mote) and is powered by batteries on-board the tool. High power requirements of such hardware necessitate frequent maintenance in changing batteries. Hence, the hardware implementation must be energy-conservative and performance-oriented. Additionally, hardware implementation of any algorithm is constrained by the limitations of the hardware. Use of specific hardware must be weighed against the precision, speed, and criticality of an algorithm's implementation. The sensor data, in addition to the decision made on the tool, may also be communicated to a centralized database server for future analysis. Constraints addressed for the implementation are use of low-power, and fast-processing hardware. In turn, the demand for low-power limits the types of processor architectures that can be deployed; therefore, the Silicon Laboratories® 8051 variant hardware has been selected for this study. In addition, since tool's mobility on the shop floor requires multi-hop, non line-of-sight radio communications capability, the Optimized Energy-Delay Sub-network Routing (OEDSR) protocol [19] has been implemented.

5.2 Hardware

The UMR mote integrated with the tool (Figure 3) is used to process and manage the flow of sensor data and decisions. The UMR mote is capable of being interfaced with virtually all analog voltage signals that have been put in the correct dynamic range. It also can be instructed by control packets to transmit data in raw or pre-processed form.

Silicon Laboratories® 8051 variant hardware has been used on the mote due its ability to provide fast 8-bit processing, low-power consumption, and ease of interfacing to peripheral hardware components. The proposed methodology and the communications protocol (OEDSR) have been implemented in the processing layer. Maxstream® XBEE

radio has an indoor/urban performance range of up to 30 m with a power output as low as 1 mW (0dBm) and typical current in the range of 45-50 mA. Such low power with effective performance criteria has helped to select the radio for wireless communications.

5.3 Routing Protocol

Certain applications in manufacturing, such as understanding process behaviors by analyzing historical data, may necessitate collection of all sensor data coming form the tool and its storage in a database residing on the base station. Such situations may overload the network. By creating an ad hoc network using the hardware from multiple tools on the shop floor will avoid the data overload on existing communication infrastructure. Hence, an energy efficient wireless routing protocol, OEDSR [19], with low end to end delay was selected for routing the decision and sensor data packets wirelessly from the tool to the server.

In OEDSR, sub-networks are formed around an event/ fault and nodes wake up in the sub-networks while the nodes elsewhere in the network are in sleep mode. For the proposed application, nodes denote the hardware on other tools. An appropriate percentage (typically 20%) of nodes in the sub-network are elected as cluster heads (CHs) based on a metric composed of available energy and relative location to an event [19] in each sub-network. Once the CHs are identified and the nodes are clustered relative to the distance from the CHs, the routing towards the server is initiated. First, the CH checks if the server is within the communication range. In such case, the data is sent directly to the server. Otherwise, the data from the CHs in the sub-network are sent over a multi-hop route to the server. The routing algorithm is fully distributed since it requires only local information for constructing routes, and is dynamic in adapting to changes in the network. Though the OEDSR protocol uses the concept of relay nodes from the

energy-delay metric from optimized energy delay routing (OEDR) [20], selection of relay nodes (RN) does not maximize the coverage of two hop neighbors. Here, the selection of a relay node is set to maximize the link cost factor, LCF_i, as given in equation (5), which includes energy, end to end delay and distance from the BS to the RN.

$$LCF_i = \frac{E_i}{D_i \cdot x_i} \tag{5}$$

where,

Di : Delay that will be incurred to reach the next hop node in range,

xi : Distance between the next hop node to the base station, and

Ei : Energy remaining at the next hop node.

In equation (5), checking the remaining energy at the next hop node increases network lifetime; the distance to the BS from the next hop node reduces the number of hops and end- to-end delay; and the delay incurred to reach the next hop node minimizes any fading channel problems. When multiple RNs are available for routing of the information, the most optimal RN is selected based on the highest LCF. These clearly show that the OEDSR protocol is an on demand routing protocol which consistently performs well in terms of energy efficiency and performance. By using this routing protocol, it is evident that the energy used for wireless communication from the tool to the server can be minimized [19]. This protocol has been successfully implemented and tested in this study.

6. EXPERIMENTATION

Three thicknesses have been tested: 3.7 mm, 5 mm, and 7.4 mm to represent normal grip, under grip, and over grip cases, respectively. The sensor data are acquired using a Universal Serial Bus based Data Acquisition Card with 8 analog input channels. The data have been sampled and stored at 5,000 samples per second for each sensor data. The proposed methodology has been implemented on a 5-layer stack mote.

After calibration of the tool and setting limits on depth, width, and peak strain based on 15-sample data set, a total 150 additional trials have been carried out for normal grip, under grip, and over grip cases on plate thicknesses of 5 mm, 7.4 mm, and 3.7 mm, respectively. The results are presented in Table 2.

Table 2. Summary of Results

Scenario	Plate Thickness (mm)	Trials	Correct Detection		False Positive		False Negative	
			Count	% Detection	Count	% Detection	Count	% Detection
Normal Grip	5	50	50	100%	0	0%	0	0%
Over Grip	3.7	50	48	96%	1	2%	1	2%
Under Grip	7.4	50	47	94%	2	4%	1	2%
TOTAL		150	145	96.7%	3	2%	2	1.3%

The results indicate a 100% correct detection of normal grip condition, while 4% of over grip cases and 6% of under grip cases are falsely detected. The false detections can be attributed to the variability caused by the tool, sensor sensitivity or human error

while operating the tool, as well as due to the size of initial training sample set (15 data points).

The false positives are those cases when the scenario is a faulty (over or under grip) one but detected as a correct (normal grip) case. These are very critical as they would pass the quality inspection for proper grip lengths even though they are not acceptable. False negatives were detected for over and under grip cases, i.e. the scenario is a faulty one (over or under grip), but detected as the wrong fault scenario (over grip being detected as under grip and vice versa). These are not as critical as the false positives since they do not pass the quality inspection and detected as fault even though the root cause diagnosis may be wrong.

However, the results in general demonstrate the performance of the proposed approach and its implementation on a prototype tool. The data also includes the drop dates of the wireless communication tool which shows that the communication is quite reliable.

7. CONCLUSIONS

In this study, unique features from the strain gage and LVDT sensor signatures are extracted to determine the quality of the fastening operations for a hand-held pull-type pneumatic tool. The feature extraction-based methodology detects normal, over, and under grip cases during the fastening process by employing simple rules; hence it is practical to implement as a real-time decision-making tool.

The experimental results have shown that over 96% of the grip lengths have been detected with 100% of the data transferred successfully via the mote. Therefore, the proposed methodology and the prototype tool have merits for further investigation and deployment. The most critical aspect of the overall scheme is to be able to properly

detect the limits on width, depth, and peak strain, which vary based on the type of the tool, fasteners, and plates.

Wireless implementation also shows that such a methodology is practical and reliable for in-process quality monitoring in a shop floor environment. Such hand-held tools are mobile resources; any type of extended wiring or bulky attachments can interfere with the fastening process. They need to be equipped with relatively small sensors, processing and communication devices so that the proposed approach can be seamlessly implemented. In this case, practicality requires wireless communications (1) to facilitate information and data flow between tools and the server, (2) for reliable data transfer through implementation of the optimized energy-delay sub-network routing (OEDSR) protocol with multi-hop, non line-of-sight radio communications capability for obstacle-rich environments. Such real-time quality control techniques reduce the amount of post-process quality control thereby saving expended capital. Similar methodologies implemented over wireless sensor networks can be very effective in other manufacturing environments as well.

Overall, the proposed architecture has merits to (1) detect and report quality problems in real-time during the process, (2) implement without complexity by extracting useful features from process signatures and performing simple rule based methodology, and (3) reduce post-process inspection, thereby improving quality while reducing cost and man power. In addition, the approach facilitates 100% data collection, for future analysis, on each fastener as opposed to traditional statistical process control techniques, which rely on sampling.

ACKNOWLEDGEMENTS

The authors also acknowledge the contribution of Jeffrey Birt (UMR) for prototyping of the tool and of James Fonda (UMR) for the implementation of the wireless communications protocol.

REFERENCES

1. J. A. Speck, *Mechanical Fastening, Joining and Assembly*. New York, NY: Marcel Dekker INC., 1997, pp 6-7.
2. Goodsmith, D., 1987, "Clamping Verification Probe," US Patent 4 649 753, Mar. 17.
3. Pekar, G., Mason, J. and Blane, M., 1989, "Portable Grip Length Indicator," US Patent 4 876 800, Oct. 31.
4. Ekdahi, M., Hanks, J., Hiller. B., LaChapelle, J., Thomas, K. and Turley M., 1998 "Fastener Verification System," US Patent 5 727 300, Mar. 17.
5. Luner, J., Hoeckelman, L. and Kleine, D., 2006, "Fastener Grip Length Selector," US Patent 7 065 897, Jun. 27.
6. Hoeckelman, L., 2006, "Clamping Fastener Grip Length Indicator," US Patent 7 070 375, Jul. 4.
7. Christian, E. and Blunck, R., 1980, "Fastener Grip Length Measuring System," US Patent 4 237 612, Dec. 9.
8. Howard, B. and Avery, J., 1997, "Real-time Fastener Measurement System," US Patent 5 673 839, Oct. 7.
9. Mauer, D., Roeser, H., Opper, R., Wojcik, A. and Schoenig, C., 2001, "Riveting System and Process for Forming a Riveted Joint," US Patent 6 276 050, Aug. 21.

10. Harlow, G. and Dise, R., 2005, "Method for Installing Blind Fasteners," US Patent 6 851 167, Feb. 8.

11. Byrne, D. and Chitty, E., 1997, "Blind Rivet Set Verification System and Method," US Patent 5 661 887, Sep. 2.

12. Weeks, G., Hull, D., Godwin, S. and Jackson, G., 2006 "Method and Apparatus for Monitoring Blind Fastener Setting," US Patent 7 024 746, Apr. 11.

13. Vanbergeijk, E., 1999, "Wireless Cycle Monitoring System for Power Tools," US Patent 5 898 379, Apr. 27.

14. Klingajay, M., Seneviratne, L. and Althoefer, K., 2003, "Identification of Threaded Fastening Parameters using the Newton Raphson Method," *Proceedings of the 2003 IEEWRSJ Intl. Conference on Intelligent Robots and Systems*, Oct., vol. 2, pp 2055-2060, 27-31.

15. Klingajay, M. and Giannoccaro, N., 2003, "Comparison between Least Square & Newton Raphson for Estimation Parameters af an Autonomous Threaded Fastenings," *IEEE Intl. Conference on Industrial Technology*, Dec., vol.1, pp 163-168, 10-12.

16. Rosenstcngel, J., Miller, I., DeSirnio, M., Derriso, M., Brown, K., Braisted, W. and Olson, S., 2004, "Detection of Fastener Failure in a Thermal Protection System Panel," *IEEE Aerospace Conference Proceedings,* Mar., vol. 4, pp 2464-2473, 06-13.

17. Giannoccaro, N. and Klingajay, M., 2004 "Identification of Threaded Fastening Parameters based on Least Square Method," *SICE Annual Conference*, Aug., vol. 3, pp 2592-2597, 04-06.

18. Seneviratne, L. and Visuwan, P., 1999, "Weightless Neural Network based Monitoring of Screw Fastenings in Automated Assembly," *Proceedings. ICONIP '99. 6th International Conference on Neural Information Processing*, Nov., vol. 1, pp 353-358, 16-20.

19. Fonda, J., Zawodniok, M., Jagannathan, S. and Watkins, S., 2006, "Development and Implementation of Optimized Energy-Delay Sub-Network Routing Protocol for Wireless Sensor Networks," *Proc. of the IEEE International Symposium on Intelligent Control*, Oct., pp. 119-124.

20. Regatte, N. and Jagannathan, S., 2005, "Optimized Energy-Delay Routing in Ad Hoc Wireless Networks," *Proc. of the World Wireless Congress*, May, 05.

PAPER II

A MULTI-INTERFACE MULTI-CHANNEL ROUTING (MMCR) PROTOCOL FOR AD HOC WIRELESS NETWORKS

Reghu Anguswamy
Engineering Management and Systems Engineering
Missouri University of Science and Technology – Rolla, Missouri, U.S.A 65409
Email: radk7@mst.edu

Maciej Zawodniok and S. Jagannathan*
Electrical and Computer Engineering
Missouri University of Science and Technology – Rolla, Missouri, U.S.A 65409
Email: mjzx9c@mst.edu , sarangap@mst.edu

corresponding author

ABSTRACT

Multiple non interfering channels are available in typical wireless networks, for example in 802.11 or 802.15.4 protocols. Capacity of the channels can be combined to achieve better performance to allow higher quality of service (QoS) wireless communication. Additionally, ever improving hardware technologies offer multiple-interface wireless nodes to be cost effective and make the multiple channel wireless communication feasible. However, existing routing protocols often are not suited to fully take advantage of available resources. Moreover, real-time applications, for example voice over wireless (VoW) systems, require consideration of multiple QoS metrics in contrast with existing multi-channel routing protocols where minimum number of hops or round trip time alone is considered.

The new multi-interface multi-channel routing (MMCR) protocol presented in this paper considers various QoS parameters such as throughput, end-to-end delay and energy utilization as a single unified cost metric for route calculations. As a consequence,

this MMCR protocol maximizes throughput while minimizing end-to-end delay and improves energy utilization. Simulation results using the Ns2 show superior performance of the MMCR over the multi-channel version of optimal link state routing protocol (OLSR).

Keywords: Wireless networks, routing protocol, multi-channel, multi-interface

I. INTRODUCTION

Wireless communications have become an integral part of life today as numerous industrial applications are being developed. However, wireless networking is prone to interference and channel problems resulting in reduced capacity. Extensive study and research has been conducted to understand and improve the capacity of wireless networks. Traditionally, communication within a network is limited to a single channel. However, capacity of the single channel is equal to the fraction of the total available bandwidth. This available bandwidth is reduced due to interference from multiple simultaneous transmissions [1]. Moreover, in multi-hop scenarios, the end-to-end performance is further reduced due to interference between adjacent hops in the same and neighboring paths [2]. As a consequence, routing protocols that utilize single channels need to be enhanced in order to accommodate multiple channels.

IEEE wireless standards, for example the IEEE 802.11b/g[3], IEEE 802.11a[4] and IEEE 802.15.4[5], offer up to 16 non-overlapping frequency channels for simultaneous communication. However, these standards do not specify how these channels should be utilized simultaneously by a particular network. A new scheme is necessary to identify and utilize free channels so that the overall network bandwidth can be increased thus improving the quality-of-service (QoS).

A wireless sensor node can be equipped with a single or multiple radios to operate in a multi-channel wireless network. In single radio scenarios, the node can transmit or listen on one channel at a given time. The node has to switch between channels to operate in the multi-channel network. However, with multiple-radios, the node is able to communicate in multiple channels simultaneously thus increasing the overall network capacity beyond the single channel bandwidth. Extensive study has been presented in [12] on the impact of number of channels and interfaces in wireless networks. There, it was shown that the capacity of multi-channel networks is dependent upon the ratio between the number of channels, c, and the number of interfaces, m. Additionally, it was shown that in a random network with up to O (log n) channels, where n is the number of nodes, interface switching delay has no effect on the capacity of the network. Further, the optimal capacity can be achieved even with single interfaces.

A multi-channel wireless network similar to a single-channel network requires topology discovery, traffic profiling, and routing [6] besides channel assignment, in order to successfully be deployed in industrial environments. Topology discovery algorithms were explored in [7] and [8] whereas traffic profiling techniques were discussed in [9] and [10]. By contrast, channel assignment and routing was combined into a single problem [11]. However as discussed in [11], channel assignment and routing are dependent upon each other: channel assignments have an impact on link bandwidths and the extent to which link transmissions interfere; hence channel assignment impacts routing in order to satisfy traffic demands. On the other hand, channel assignment and routing can be considered as separate problems as in [6].

Several papers address channel assignment in a dynamic fashion. However, the channel switching introduces latency due to reconfiguration of transceiver on the particular radio interface due to added communication delay. The persistent technology improvements reduce the switching delay, for example channel switching for WiFi transceiver (802.11) may be close to 80 microseconds [14]. Al though small, this latency has to be explicitly considered during routing and congestion.

The existing routing protocols for multi-channel wireless networks [11,12,13-15, 20-22] do not consider the energy utilization and channel state of the mobile nodes. These protocols generally deal with a single quality-of-service (QoS) metric such as throughput or delay or round-trip time.

A routing protocol utilizing multiple channels with a single interface in [14, 20, 21] has been developed where the channel assignment and routing were decoupled in [14]. Here the channel assignment is performed regardless of network traffic. On the other hand, the channel can be assigned using per-flow basis, i.e. all the nodes in a particular path use the same channel. This constrains that two consecutive nodes on a path cannot switch channels, one of them has to stay in one channel; a node must notify its neighbors in a path whenever it switches channels; a node can only switch between a small number of channels (such as two), although many more channels are available; and nodes may not switch channels too frequently on a per-packet basis.

In the second approach, the nodes are locked to certain channels thus limiting the bandwidth utilization and not offering an optimal solution. In [20], a link layer solution based on time division multiple access (TDMA) of multiple channels, with a single interface known as the Slotted Seeded Channel Hopping (SSCH) was presented. In this

scheme, the nodes hop from one channel to another based on a pseudo-random sequence at the receiver. The receiver communicates this information to the sending node requesting it to switch channels. However, this scheme requires high degree of synchronization for time slotting and effective node scheduling to be in the same continuous sequence of channels.

Many multi-radio interface based protocols have also been proposed in [13, 22]. In [13], a new metric named Expected Transmission Time (ETT)/Weighted Cumulative-ETT was presented for multi-radio multi-hop wireless networks in order to identify a high throughput path between a source and a destination. A routing protocol namely multi-radio link quality source routing (MR-LQSR) was presented with a performance metric that renders a tradeoff between throughput and delay. However, this protocol is only effective for wireless mesh networks with static nodes and may not be suitable for mobile ad hoc networks since energy efficiency of the nodes for routing are not considered. The optimized link state routing (OLSR) has been modified into different flavors for the multi-channel scenario. Multi Channel OLSR (m-OLSR) presented in [26] uses a modified routing messages with number of hops as the routing metric. However, a route with the minimum number of hops need not be necessarily optimal for maximizing throughput or minimizing end-to-end delays as observed even for single channel routing schemes.

The basic challenge considered in developing the new routing protocol in multi-channel environment involves the selection of the best route from the source to the destination based on a more appropriate metric. The routing metric must consider the three major measures of QoS namely the throughput, energy efficiency and the end to

end delay for data transfer even during congestion. In order to fully exploit the advantages of the multi-channel environment, the route elected must be in multiple channels over multiple hops. Additionally, the routing protocol must also take into consideration the amount of overhead being added for communication while discovering routes in the shortest possible time.

Hence, the need for effective multi-channel routing protocols for mobile ad hoc wireless networks has been growing with considerations to enhance bandwidth utilization while minimizing energy efficiency and end-to-end delay. Therefore, a proactive routing protocol is introduced here that works independent of channel assignment. The protocol is based on the concept of multi-point relays (MPRs) of [16]. The protocol aims to maximize the throughput and energy efficiency while minimizing the end to end delay.

A node may be equipped with multiple radios capable of receiving data over multiple non-interfering channels. Now, the challenge arises as to how a node chooses the best channel to send data to a node with multiple listening radios. Also, sending data over a single channel to such nodes may not be optimal due to channel contention from other sources or due to limited bandwidth over a channel. The transmitting node must be able to balance the load among the available channels which is what is being accomplished by optimizing the bandwidth available between the nodes.

II. THE PROPOSED ROUTING PROTOCOL

Before introducing the routing protocol, the channel allocation scheme is assumed to be receiver based channel allocation where each node is assigned a dedicated non-interfering channel for receiving data. The nodes are assumed to be equipped with multi-radio interface (two radios) - one radio for incoming data on a dedicated channel, and the

other radio for outgoing data which switches between channels according to the incoming channel of the next hop node. The following definitions are needed before we proceed.

Nomenclature:

N : Set of nodes in the network

s : Source node

d : Destination node

$N(s)$: Set of one-hop neighbors of node s

$N^2(s)$: Set of two-hop neighbors of node s

$MPR(s)$: Selected Multipoint Relay (MPR) set of node s

A. Routing Metric

Utilization metric (U_{s,n_2}^{MPR}) of the link from node s to a two-hop neighbor node n_2 through the chosen MPR (n_1) is given by:

$$U_{s,n_2}^{MPR} = (B.F. * E.U.)/D. \quad (1)$$

$$B.F. = B_A / B_S. \quad (2)$$

$$E.U. = E_A^{n1} / E_{TX}^{n1->n2}. \quad (3)$$

where $B.F.$ is a bandwidth factor between nodes s and MPR (n_1), B_A is an available incoming bandwidth at the MPR (n_1), B_S is an expected outgoing bandwidth at the source node (s), $E.U.$ is an energy utilization between MPR (n_1) and n_2, E_A^{n1} is an available energy at the MPR (n_1) in Joules, $E_{TX}^{n1->n2}$ is a transmission power from n_1 to n_2, and D is an end to end delay from node s to node n_1 in seconds.

The bandwidth factor ensures that there is sufficient bandwidth for data transfer. Also, a route is selected if and only the bandwidth factor of all the links on the path is greater than one, so that there is only one route is associated with a flow at any given instant and thus guarantees service only if sufficient bandwidth is available. However, the

route may be dynamic with periodic updates of the MOR set. The energy utilization is a measure of energy depletion due to usage and hence ensures energy efficiency. The end-to-end delay is one of the QoS metric for route selection. The unit of the utilization factor can be seen as bytes/sec which is a direct measure of the throughput of the link. The routing scheme is introduced next.

B. The Protocol Algorithm

1. [Neighbor Sensing] Each node in the network transmits HELLO packets to its neighbors. The HELLO packets are similar to the one used in the implementation of OLSR as in [17] with some modifications. The header of the HELLO packet is modified to include the transmission time. The node receiving the HELLO packet can extract the delay by using the stamped transmission time of the HELLO packet header; however, this requires time synchronization between the nodes. The HELLO packets contain the list of its neighbors and the energy utilization for each of these neighbors. The HELLO packets also contain information about the channels the node can receive data and the available bandwidth in that channel. This information is used by the receiving node to calculate the bandwidth factor of that channel to that node. When HELLO packets are received, each node updates this information on bandwidth available, energy factor and the delay of the links from their neighbors in the 'neighbor table'.
2. [Multipoint Relay Selection] For each node in the network, its 'neighbor table' is used to select the multipoint relay nodes from the one-hop neighbors to reach all the two-hop neighbors with minimum cost given by equation (1).

a) Variable set of MPRs – The set of MPRs to reach the two hop neighbors is variable, since the optimal set varies with time and traffic.

b) A route is discarded only in the case of any link failures on the path from the source to the destination.

3. [Topology Information Declaration] Upon selection as a MPR, nodes transmit TC messages, consisting of link utilization factor to all the nodes in the network through a broadcast. Upon receiving the TC messages, each node in the network records the information in the 'topology table'.

4. [Routing Table Calculation] Each node in the network proactively computes the routes to all the destination nodes in the network by using the 'neighbor table' and the 'topology table' using the information at the node. The protocol selects the best route with the least link cost metric with the constraint that the bandwidth factor is always greater than one for all the links on the path. The cost factor for a route with k intermediate MPRs nodes in the path is given by

$$C_{s,d} = \sum\left(C_{s,n_2}^{n1}, C_{n1,n_3}^{n2}, \ldots\ldots, C_{n_{k-2},n_k}^{n_{k-1}}, C_{n_{k-1},d}^{n_k}\right) \quad (4)$$

where

C_{s,n_2}^{MPR}: Cost metric of the link from node s to node n_2 through the chosen MPR (n_1) and $n_2 \in N^2(s)$; is given by

$$C_{s,n_2}^{MPR} = 1/U_{s,n_2}^{MPR} \quad (5)$$

C. Network overhead

Compared to the OLSR, MMCR has a slightly higher network overhead which can be explained using two factors. First, the number of MPRs selected by the MMCR

will be greater than or equal to that selected by the OLSR. Thus, the number of nodes transmitting the topology control (TC) messages will be greater than or equal to that sent by the OLSR.

The second factor that contributes to the network overhead is due to the additional bytes introduced in the routing messages (HELLO and TC) for the OLSR. As a MPR-based routing protocol, MMCR begins with the neighbor sensing by sending HELLO packets. The HELLO packets are similar to the one used in the implementation of OLSR with some modifications. The header of the HELLO packet is modified to include the transmission time. In HELLO packets, the header is increased by 4 bytes to include the transmitting time of the packet. The data portion of the HELLO messages includes the information of the one hop neighbors of the sending node. In OLSR, only the node ids are included as it considers only minimum hops for routing calculations.

For MMCR, in addition to the node ids, information regarding the delay, bandwidth available at the node and the energy required to send a packet to the one hop neighbor are included. The Topology Control (TC) messages are also modified for the MMCR. The header remains the same that includes the number of hops. The data portion of the TC message has the information for each MPR-selector: delay and energy for transmitting a packet, are included. Data portion of the HELLO message include sections with each section containing the information for each one hop neighbor. For each section or each one hop neighbor, information on the bandwidth available at the node, the energy required to send a packet to the one hop neighbor and the delay are included. The bandwidth available and the energy information are used for calculating the bandwidth factor and energy utilization respectively.

In the simulations, maximum bandwidth available is assumed to be 0.7Mbps and the bandwidth of the source is assumed to be 300kbps. Thus, the bandwidth factor has a range of 0 to 250 and the bandwidth available can be represented in the HELLO section using one byte. Similarly, for the energy utilization the maximum energy (initial energy of the node) is 100J and the transmission energy is typically in the range of 0.01 to 0.218. Thus, the energy information is included with an addition byte that represents the transmission energy scaled to the range of 10 to 218. The delay information is also represented using a byte with the delay varying from 0.001 to 0.25 secs. The comparison of the overhead for HELLO packets is as shown in Table 1.

Table 1. HELLO packets for MMCR and OLSR

HELLO_HEADER			
OLSR		MMCR	
Data	Size (bytes)	Data	Size (bytes)
msg_seq	2	msg_seq	2
mpr_seq	2	mpr_seq	2
		start_time	4
HELLO_SECTION			
OLSR		MMCR	
Data	Size (bytes)	Data	Size (bytes)
link_type	1	link_type	1
Reserved	1	Reserved	1
Length	2	Length	2
		Delay	1
		bandwidth	1
		Energy	1

In TC packets, the header in MMCR is similar to that of the OLSR and therefore no overhead is introduced. Data portion of the TC message include sections with each section containing the information for the nodes which have selected the current node as the MPR. For each section, information on the bandwidth available at the node, the energy available at the node and the delay are included. The bandwidth available and delay are represented using additional bytes similar to the HELLO packet. The energy available and the energy for transmission are represented using an additional byte for the energy utilization factor. The comparison of the TC section for OLSR and MMCR is shown in Table 2.

Table 2. TC section comparison for OLSR and MMCR

TC_SECTION			
OLSR		MMCR	
Data	Size (bytes)	Data	Size (bytes)
node_id	1	node_id	1
		delay	1
		bandwidth	1
		energy_utilization	1

C. Multiple Channels over a Link

A node may be equipped with radios capable of receiving data over multiple non-interfering channels. The bandwidth available for each receiving channel at each node is sent via HELLO packets to its neighbor nodes. The neighbor node receiving these HELLO packets stores the available bandwidth information for each of these channels. The available bandwidth at each node is the sum of the available channel bandwidths over all the channels.

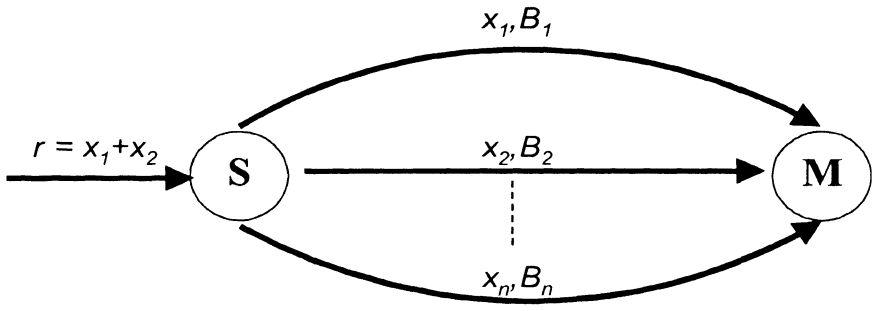

Figure 1. MPR node *M* has *n* receiving channels with bandwidths *B1, B2 ... Bn*

The node with multiple receiving channels as shown in Figure 1, when selected as a MPR, is now capable of receiving data over multiple channels. The receiving node may be already receiving data from a different source through a channel and hence, the bandwidth available among the receiving channels may be different. So the data must be sent be in a balanced mode among the various channels for optimal performance. Mathematical analysis of balancing the load among different channels is presented next.

Bertsekas and and Gallager [23] have presented the characterization of optimal routing for directing traffic along paths which are shortest with respect to some link costs that depend on the flows carried by the links. The cost function for a route can be expressed as

$$\sum_{i,j} C_{ij(}X_{ij)} \tag{6}$$

where C_{ij} is a cost function for link (i,j) as a function of the total X_{ij} over the link

$$Xij = \sum b_p \tag{7}$$

and b_p is a flow through a path containing the link (i,j)

The problem of identifying the best routing path now reduces to minimizing (6) and (7). According to [23] the optimal set of flows (b') is achieved when the traffic is split through the following constraint

$$\sum_{p \in P_w} [\partial C(b') / \partial b_p](b_p - b') \geq 0 \tag{8}$$

The cost function in the presented routing protocol is inversely proportional to the bandwidth factor (B.F.) which is function of the flow between the links. Thus, the cost function is obtained as

$$Cn(B.F.) = k / B.F._n = k * B_s / B_A \tag{9}$$

where k is a constant, and

$$B_s = b \tag{10}$$

$$B_A = B - b \tag{11}$$

where B is channel capacity.

Consider a node consisting of n receiving channels having bandwidths B_1, B_2 ... B_n such that $B_1 > B_2 > \ldots > B_n$ and let b_1, b_2, ..., b_n be the bandwidths allocated to each channel by the transmitting node. From equations (8) – (10), optimal solution is achieved for k available channels when the following condition (refer APPENDIX A for proof based on extending the work given in [23]) is satisfied for all $j \in [1, k-1]$ as

$$\frac{B_j}{(B_j - b_j)^2} - \sum_{\substack{i=1 \\ i \neq j}}^{k-1} \frac{Bi}{(Bi - b + \sum_{\substack{m=1 \\ m \neq i}}^{k-1} b_i)^2} \leq \frac{1}{B_k} \tag{12}$$

When homogeneous network with similar physical interfaces for each channel is considered, the constraint (12) becomes equal capacity assignment for all channels. In

such cases, optimal solution is achieved when the link bandwidth is equally allocated among all the available channels on the link.

III. OPTIMALITY ANALYSIS

The optimality analysis shows that the routing protocol presented is optimal in all scenarios. The optimal route is analyzed and defined as the route with the minimum overall cost defined in the routing protocol. The analysis is as presented below:

Assumption 1: *If the one-hop neighbor of a node s, has no direct link to at least one of the two-hop neighbors of s, then it is not on the optimal path from s to its two-hop neighbors. However, in order to reach a two-hop neighbor from s through such a node, the path has to go through another one-hop neighbor which has a direct link to the two-hop neighbor.*

Corollaries 1 and 2 present the case when the destination nodes have no direct link to the source node and are at a two-hop distance from the source node. Corollary 1 is in line with [19].

Corollary 1: "The MPR selection based on the utilization metric – based MPR selection provides the optimal route from a node to its two-hop neighbor."

Proof: Case I: When the node d in $N^2(s)$ has only one neighbor from $N(s)$, then that node in $N(s)$ is selected as the MPR node. In this case, there is only one path from the node s to d in $N^2(s)$. Hence, the multipoint relay selection algorithm will select this as the best route between s and the two-hop neighbor d in $N^2(s)$.

Case II: When the node d in $N^2(s)$ has more than one neighbor in $N(s)$, the MPR nodes are selected based on the multipoint relay selection criteria.

Consider a node s whose one-hop neighbors are given by $N(s)$, and a particular node d in $N^2(s)$ with multiple nodes $n_1, n_2, ..., n_k$ $(k > 1)$ belonging to $N(s)$ as its neighbors. Let the cost factor to reach d through k^{th} one-hop neighbors from s be $C_{s,d}^{m_k}$. According to the MPR selection criteria, the multipoint relay node to cover d from s is selected as the node n_i with cost factor of:

MIN $[C_{s,d}^{m_1}, C_{s,d}^{m_2}, ..., C_{s,d}^{m_{k-1}}, C_{s,d}^{m_k}]$

Hence, the MPR selection criteria will result in optimal route from s to its two-hop neighbors in $N^2(s)$ based on the cost metric.

Corollary 2: "The set of MPRs selected for its two-hop neighbors is optimal"

Proof: Let, there are k one-hop neighbors and j two-hop neighbors for a source s. Let, the optimal set of MPRs be $[m_1, m_2, ..., m_k]$ and the optimal set of the cost factor associated with the MPRs be represented as

$[C_{s,n1}^{m_1}, C_{s,n2}^{m_1}, C_{s,n3}^{m_2} ....., C_{s,nj-1}^{m_k}, C_{s,nj}^{m_k}]$.

Let us now introduce a new one-hop neighbor, m_{k+1} with a direct link to node n_j and its cost factor be $C_{s,nj}^{m_{k+1}}$.

If $\quad C_{s,nj}^{m_{k+1}} < C_{s,nj}^{m_k}$,

Then, by corollary 1, m_{k+1} becomes a new chosen MPR to reach the node n_j, and is added to the set of MPRs. Consequently, the cost factor set for the MPRs becomes:

$[C_{s,n1}^{m_1}, C_{s,n2}^{m_1}, C_{s,n3}^{m_2}, ..., C_{s,nj-1}^{m_k}, C_{s,nj}^{m_{k+1}}]$,

which forms the new optimal set of MPRs.

Else

By Corollary 1, the m_{k+1} is not chosen as a new MPR and the set of MPRs remain unchanged since it is optimal.

Corollary 3 and Theorem 1 discuss the optimality of route selection through the MPRs. The intermediate nodes are selected MPRs by the previous nodes on the path.

Corollary 3: "The intermediate nodes on the optimal path are selected as multipoint relays by the previous nodes on the path."

Proof: A node in the route may not be selected as the MPR by the previous node if the node does not provide connection to that node's two-hop neighbors or the node does not meet the MPR selection criteria. The node in $N(s)$ of the previous node s, does not provide connection to any node in $N^2(s)$. Consider the Figure 2 shown below. Node n_2 only connects to node s's one-hop neighbor n_1. The two possible paths from s to d are $s -> n_1 -> d$ and $s -> n_2 -> n_1 -> d$. According to Assumption 1, n_2 is not on the optimal path from s to d.

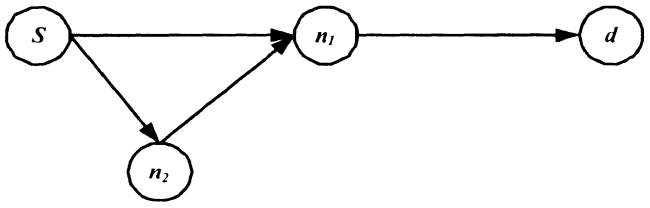

Figure 2. Destination at two-hops

Based on the Corollaries 1, 2 and 3 it can be shown the routing protocol always selects the optimal route in terms of the cost metric presented.

Theorem 1: The routing protocol selects the optimal route based on the cost metric between any source-destination pair.

Proof: There is an optimal path from source to destination such that all the intermediate nodes on the path are selected as MPRs by their previous nodes on the same path.

Consider the Figure 3 shown below. Without loss of generality, we suppose that in an optimal path, $s -> n_1 -> n_2 -> \ldots -> n_k -> n_{k+1} -> \ldots -> d$, there are nodes in the route which are not selected as MPRs by their previous nodes. Also, based on the result of corollary 3, we can assume that for each node on the path, its next node on the path is its one-hop neighbor, and the node two hops away from it is its two-hop neighbor. For example, n_1 is s's one-hop neighbor and n_{k+2} is n_k's two-hop neighbor. Consider the following two situations:

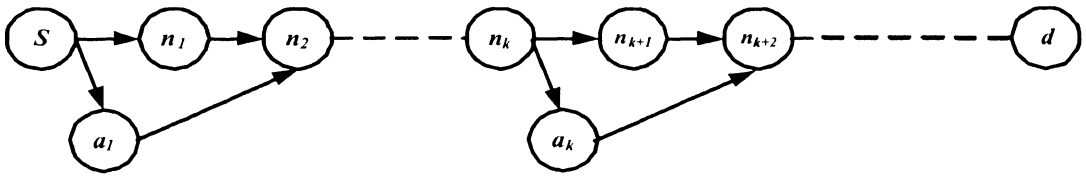

Figure 3. The optimal route scenario between source and destination nodes

1. Suppose that on the optimal route, the first intermediate node n_1 is not selected as MPR by source s. However, n_2 is the two-hop neighbor of s. Based on the basic idea of MPR selection that all the two-hop neighbors of s must be covered by its MPR set, s must have another neighbor a_1, which is selected as its MPR, and is connected to n_2. According to the MPR selection criteria and corollaries 1 and 2, s selects a_1 instead of n_1 as its MPR since the cost to reach n_2 using a_1 is less than or equal to the cost to reach n_2 using n_1.
2. Since route $s -> n_1 -> n_2 -> \ldots -> d$ is an optimal path, => $s -> a_1 -> n_2 -> \ldots -> d$ is also an optimal path - the utilization of the path is the maximum.

This implies that the source's MPR are on the optimal path. Assume that on the optimal route $s -> n_1 -> n_2 -> \ldots -> n_k -> n_{k+1} -> \ldots -> d$, all the nodes on segment $n_1 -> \ldots -> n_k$ are selected as MPR by their previous node, we now prove that the next hop node of n_k on the optimal route is n_k 's MPR.

Suppose that n_{k+1} is not n_k 's MPR. Same as in I, n_{k+2} is the two-hop neighbor of n_k, so n_k must have another neighbor a_k, which is the MPR of n_k and has connection to n_{k+2}. Again, n_k selects a_k instead of n_{k+1} as its MPR since the cost to reach n_{k+2} using a_k is less than or equal to the cost to reach n_{k+2} using n_{k+1}.

Since route $s -> \ldots -> n_k -> n_{k+1} -> n_{k+2} -> \ldots -> d$ is an optimal path, => $s -> \ldots -> n_k -> a_k -> n_{k+2} -> \ldots -> d$ is also an optimal path.

This implies that in an optimal route, the $(k+1)^{th}$ intermediate node is the MPR of the $(k)^{th}$ intermediate node and all the intermediate nodes of an optimal path are MPRs of the previous node. Thus, the routing protocol selects the best optimal route based on the cost metric for the route between any source-destination pair

IV. RESULTS AND DISCUSSION

The routing protocol was analyzed in Ns2 simulations using IEEE 802.11 with CBR/UDP sources. The Ns2 version 2.30 was extended with multi-channel and multi-interface capability based on the guidelines provided in [24, 25]. The nodes have multiple interfaces, one of them dedicated for transmission. 10 independent non-interfering channels are used and a node is assigned a fixed channel through another dedicated interface to receive data for the entire simulation time period. The packet size is set to

210 bytes and the two-ray ground propagation model is utilized. Priority queue with queuing buffer of size 50 is used.

OLSR and OEDR protocol for single channel was modified for the multi-channel environment to m-OLSR and m-OEDR. The routing packets (HELLO and TC) are not modified and remain the same, but they are broadcast in all the available channels. The network overhead is defined as the total bits sent per node (HELLO and TC packets only) in unit time. Energy efficiency is defined as the number of packets received over the energy spent by all the nodes in the network. The performance of the multi-channel routing scheme is compared with m-OEDR and m-OLSR protocols for multi-channel environments. The performance is analyzed in terms of average received throughput, average dropped throughput, average end-to-end delay and energy efficiency. The simulations are run for random 10 iterations and data are averaged over these 10 iterations for each data point.

A. Static topology – varying number of flows

In this scenario, 32 nodes are fixed in a flat grid of size 1000m x 1000m in a mesh topology. The packets are sent at a rate of 82kbps. The number of flows is varied in order to test scalability of the routing protocols. Performance of the proposed scheme is compared against the multi-channel versions of OEDR and OLSR (m-OEDR and m-OLSR). The throughput, dropped packets and end-to-end delays are as shown in Figures 4, 5 and 6. The energy efficiency is given in Table 3, and the network overhead is given in Table 4.

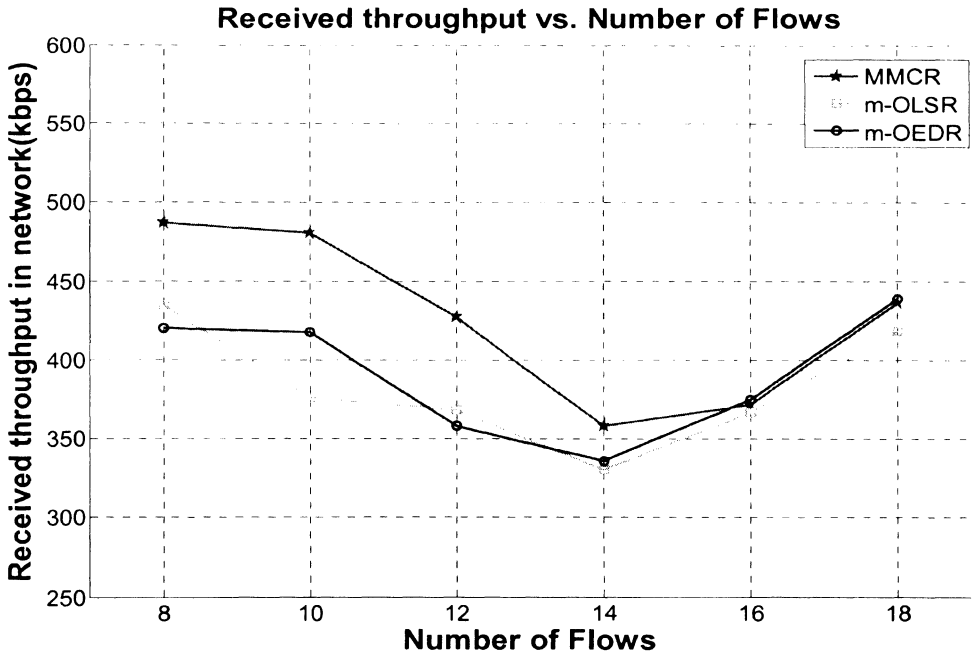

Figure 4. Received throughput vs. number of flows

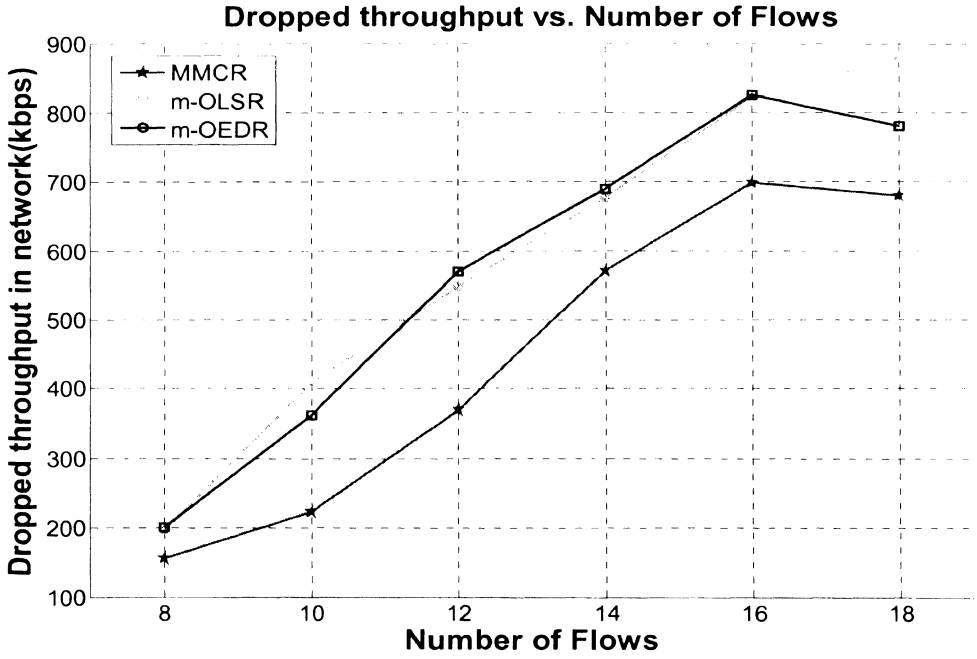

Figure 5. Dropped throughput vs. number of flows

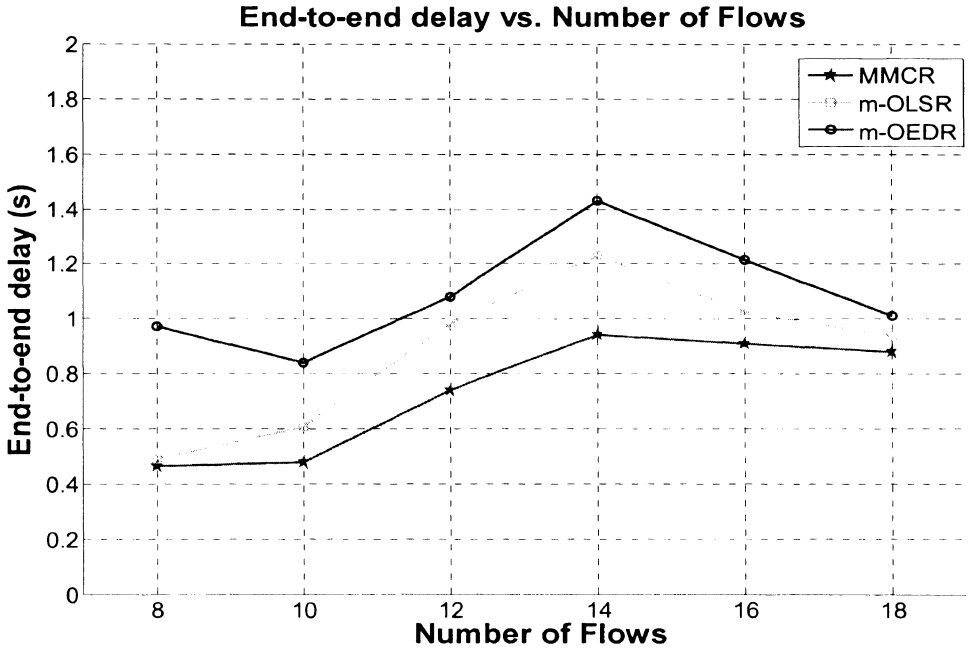

Figure 6. End-to-end delay vs. number of flows

Table 3 Energy efficiency for varying number of flows

Number of flows	Energy Efficiency (pkt/J)		
	MMCR	m-OLSR	m-OEDR
8	21.3	21	17.2
10	20.6	17.5	15.1
12	16.5	14.7	13.3
14	12.4	11.3	11.1
16	13.9	13.4	12.2
18	18	15.2	15.4

Table 4. Network overhead

Overhead	MMCR	m-OLSR	m-OEDR
Network overhead (kbps per node)	1.02	0.89	2.05
Number of MPRs selected	30-32	28	30-32

MMCR outperforms the other protocols in terms of throughput regardless of the number of flows since it selects the paths that will reduce end-to-end delay and improve throughput. On an average, MMCR increases throughput by 11.6% over m-OLSR, and 27.4% over the m-OEDR. Additionally, MMCR ensures lower end-to-end delay. On an average, MMCR experiences 16.2% less end-to-end delay when compared with m-OLSR, and by 32.5% when compared with m-OEDR. The MMCR is also better in energy efficiency by 10.4% and 18% as compared to m-OLSR and m-OEDR respectively.

The number of MPRs selected by the MMCR is always greater than the m-OLSR and selects 30 to 32 nodes as MPR thereby increasing the network overhead for MMCR. However, MMCR still performs better as it chooses routes with the bandwidth factor constraint being greater than one and hence improves the throughput. The congestion in the network is increased as the number of flows in the network increases as observed in these figures. From Figures 4 and 5, it can be observed that the received throughput decreases and the dropped packets increase due to more congestion resulting in higher number of collisions. The increase in the end-to-end delay in the network as observed in Figure 6 also gives an indication of the higher congestion. The m-OEDR protocol performs lower since the delay is only considered and this factor influences the decision on route generation as compared to MMCR which has bandwidth factor consideration to get around congested nodes. The energy spent by the network for MMCR is comparable to m-OLSR and m-OEDR, however with higher throughput the energy efficiency achieved is higher. If the number of flows continues to increase, the network reaches a steady state due to which the throughput increases and end to end delay decreases.

The number of hops may be increased to avoid high congestion for MMCR, however, the end-to-end delay is also decreased due to these paths around the congested nodes lowering queuing delay and collisions. This indicates that the proposed protocol is able to take advantage of the available capacity of the multiple channels in a more effective way than the other schemes. As a result, with an average higher received throughput, the energy efficiency achieved is also higher.

B. Static topology – varying load per flow

In this scenario, 32 nodes are fixed in a flat grid of size 1000m x 1000m in a mesh topology. Flows are introduced randomly and the number of flows introduced during the simulation is fixed to 10. The data rate of a flow is varied in order to observe the impact of the network congestion on performance of the MMCR, m-OEDR, and m-OLSR protocols. The throughput, dropped packets and end-to-end delay results are illustrated in Figures 7, 8 and 9. The energy efficiency is given in Table 5.

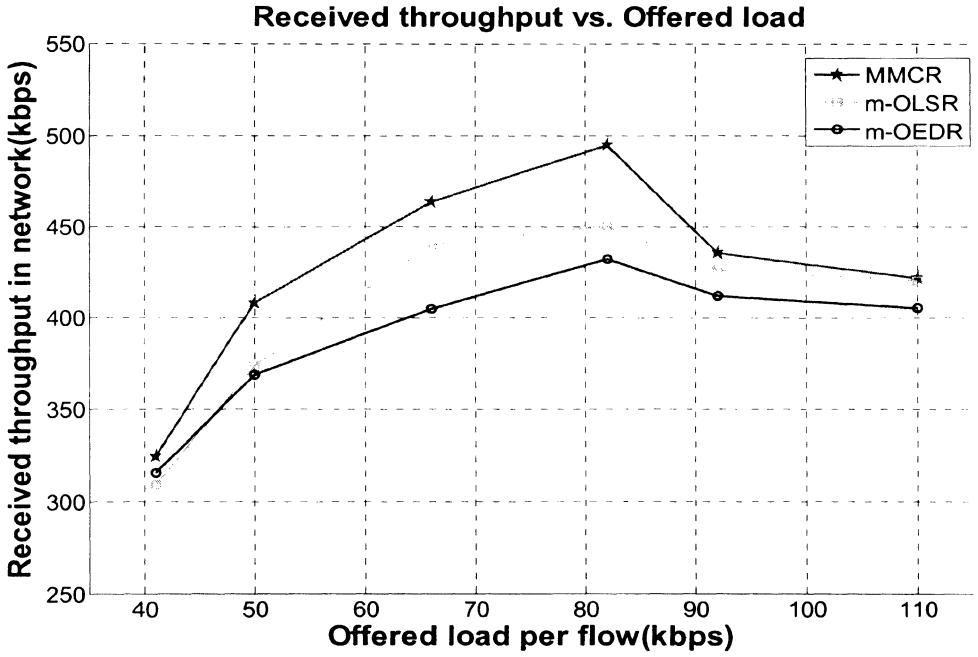

Figure 7. Received throughput vs. offered load per flow

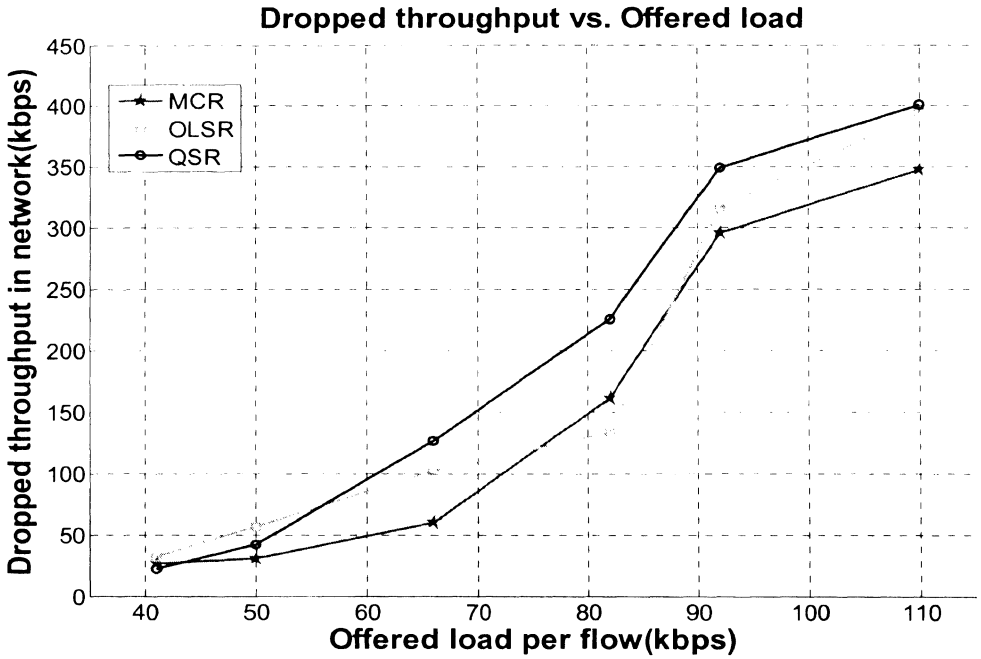

Figure 8. Dropped throughput vs. offered load per flow

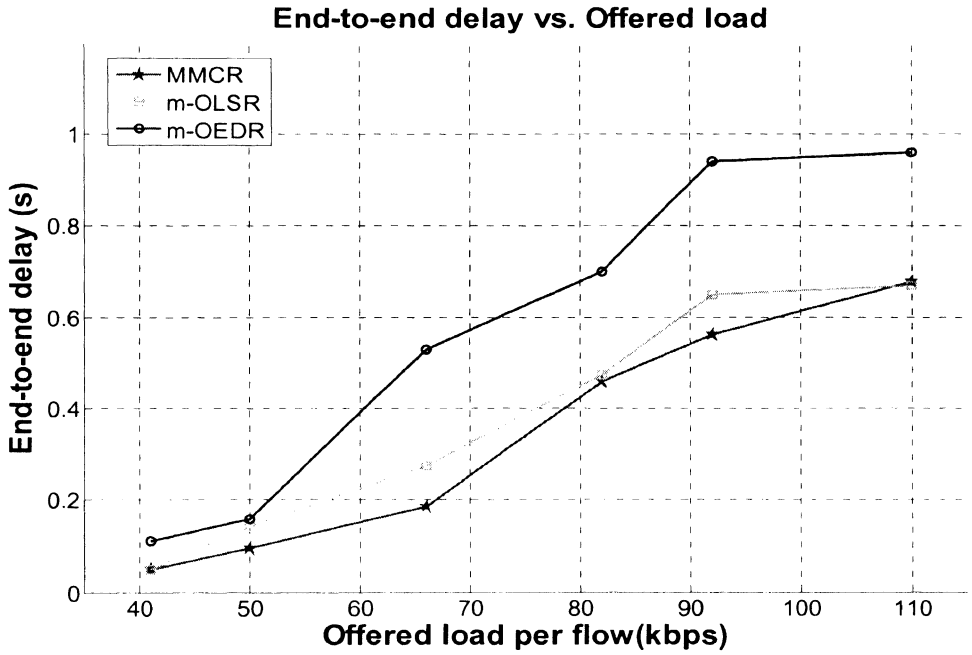

Figure 9. End-to-end delay vs. offered load per flow

Table 5. Energy Efficiency for varying offered load per flow

Offered load (kbps)	Energy Efficiency (pkt/J)		
	MMCR	m-OLSR	m-OEDR
41	21.3	22.5	17.3
50	22.3	21.4	17.7
66	23.1	23.6	18.2
82	21.7	21.4	16.5
92	17.8	18.1	17.1
110	19.9	20	16.9

In this scenario too, MMCR outperforms the other protocols in terms of throughput regardless of the offered load per flow. The MMCR selects path based on bandwidth factor at each node, thus avoiding congested nodes where the bandwidth factor is low. As a result, MMCR increases average throughput by 5.3% over m-OLSR, and 8.9% over the m-OEDR. Additionally, MMCR ensures lower end-to-end delay. On

an average, MMCR experiences end-to-end delay lower by 10.2% when compared with m-OLSR, and 40% when compared with m-OEDR. The MMCR has energy efficiency lower by 0.7% as compared to m-OLSR and higher by 21.6% as compared to m-OEDR. At higher data rates the network becomes more congested and MMCR chooses the route with lower delay as well as routes with bandwidth factor greater than 1. This is evident in the improvement achieved for lower end to end delay and higher received throughput.

From Figures 7 and 8, at a data rate of 82kbps per flow, the received throughput reaches the peak and then drops for higher data rates because the congestion in the network is increased causing more number of collisions. At 82 kbps, the network reaches the optimal performance in terms of the load the network can handle for this topology. The congestion in the network is also evident from the end-to-end delays shown in Figure 9 where it is very high for high traffic loads in the network. In this scenario, the MMCR has identified the routes that minimize the delay and there are no routes or nodes left to route the packets. Therefore the overall throughput decreases while the end to end delay increases. However, the overall throughput is higher than the other two protocols. Al though the energy spent by MMCR is comparable with that of m-OLSR, the energy efficiency of MMCR achieved is still higher due to increased throughput and fewer collisions.

C. Mobile topology – varying load per flow

In this scenario, 32 nodes are placed in a flat grid of size 1000m x 1000m in a mesh topology. Ten flows with a data rate of 82kbps are introduced. The nodes are allowed to move in a random manner with a specified maximum speed. The routing protocol is analyzed and compared to the multi-channel m-OEDR and m-OLSR. The

throughput, dropped packets and end-to-end delays are shown in Figures 10, 11 and 12. The energy efficiency is given in Table 6.

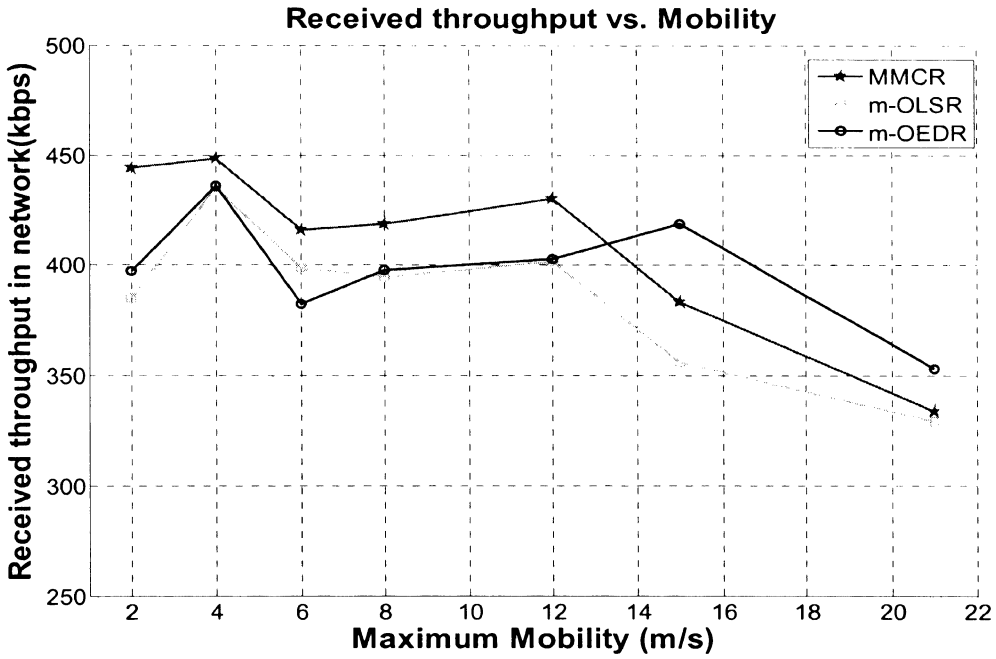

Figure 10. Received throughput vs. mobility

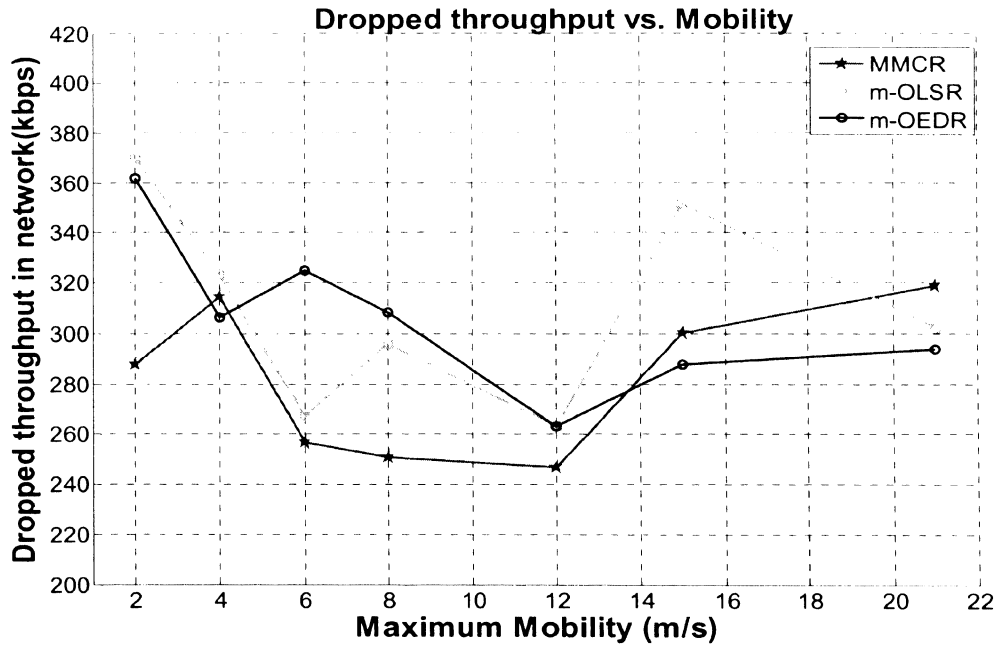

Figure 11. Dropped throughput vs. mobility

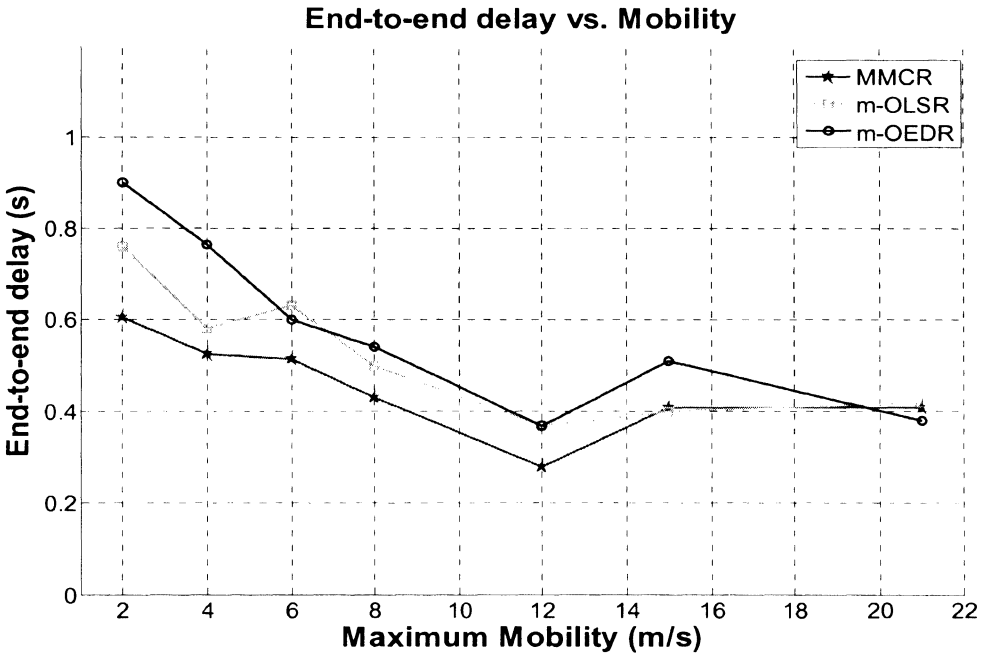

Figure 12. End-to-end delay vs. mobility

Table 6. Energy efficiency for varying mobility

Mobility (m/s)	Energy Efficiency (pkt/J)		
	MMCR	m-OLSR	m-OEDR
2	19.1	17.6	15.8
4	20.8	21	16.9
6	17.8	17.4	13.6
8	20.4	18.7	15.3
12	24.8	24.7	19.7
15	21.3	19.3	19.8
21	19.7	20.7	19

MMCR outperforms the other protocols for an average mobility of 12 m/s or less in terms of average received throughput and average end-to-end delay. On an average, MMCR increases throughput by 6.5% over m-OLSR, and 3.2% over the m-OEDR while it ensures lower end-to-end delay. On an average, MMCR lowers end-to-end delay by

13.2% when compared with m-OLSR and by 21.9% when compared with m-OEDR. The MMCR also achieves higher energy efficiency of 3.2% and 19.8% as compared to m-OLSR and m-OEDR respectively.

In mobile networks, when the nodes are in random motion the network connectivity becomes an issue. Some nodes may move farther losing network connectivity. From Figures 10 and 11, the throughput of the network is observed to be fairly consistent for node mobility less than 12m/s. However, at high mobility all the protocols exhibit a drop in their performance. At high node mobility, m-OEDR performs marginally better than MMCR. This is because the MMCR has the bandwidth factor constraint and is unable to cope up with the changes in topology as compared to m-OEDR which considers only the delay and energy parameters. Since MMCR has higher received throughput for mobility upto 15 m/s, the energy efficiency achieved is also higher. At 21 m/s due to frequent topology changes when MMCR does not perform well in terms of throughput, the energy efficiency also reduced.

D. Mobile topology – varying node density

In this scenario, nodes are placed in a flat grid of size 1000m x 1000m in a mesh topology. The number of nodes are varied as 32, 48, 60, 72 and 82 with the number of flows introduced being 12, 16, 20, 24 and 28 respectively. The nodes are allowed to move in a random manner with a maximum speed of 6 m/s. The routing protocol is analyzed and compared to the multi-channel m-OEDR and m-OLSR. The throughput and end-to-end delays are shown in Figures 13, 14 and 15. The energy efficiency is displayed in Table 7 and the network overhead in Table 8.

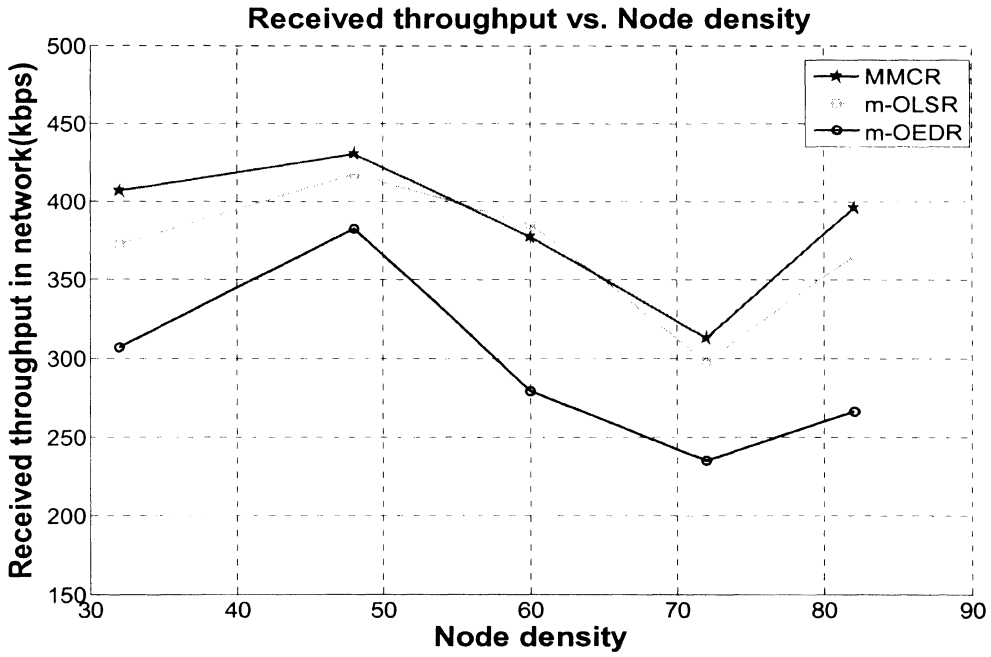

Figure 13. Received throughput vs. node density

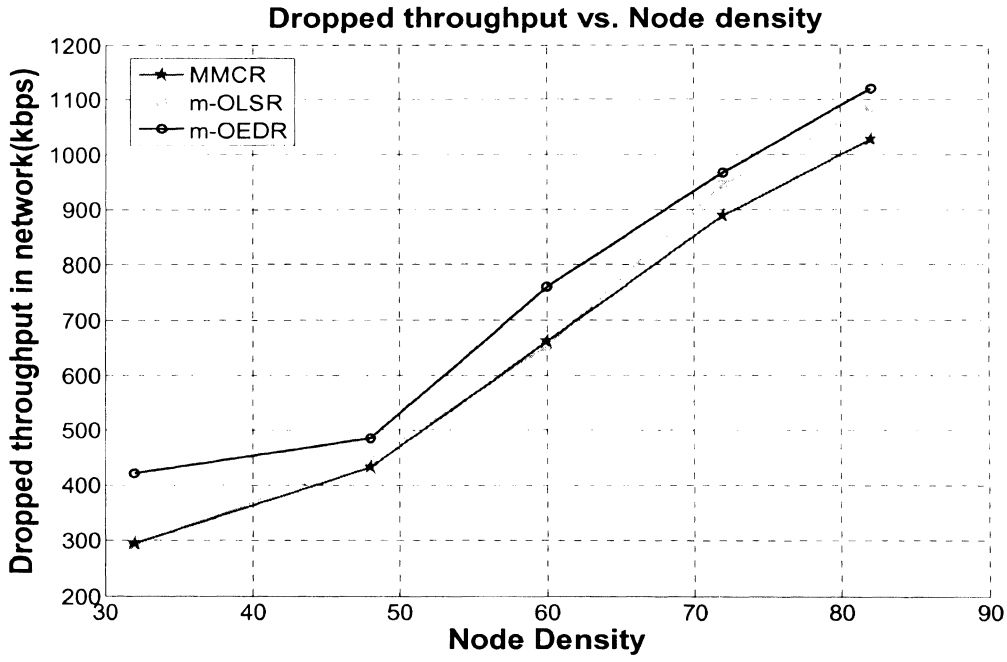

Figure 14. Dropped throughput vs. Node density

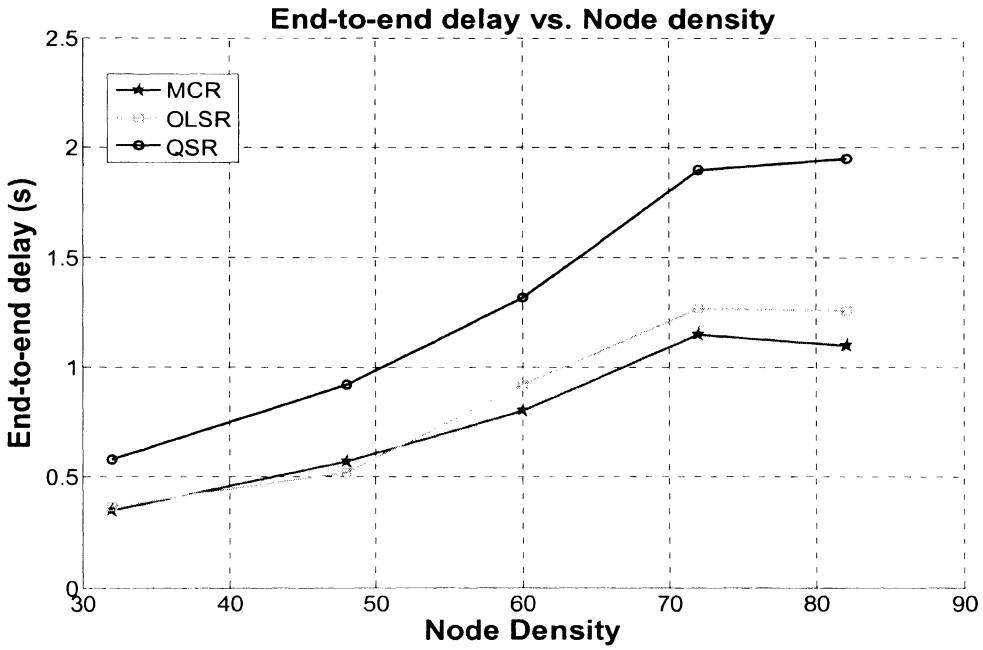

Figure 15. End-to-end delay vs. node density

Table 7. Energy efficiency for varying node density

Node density	Energy Efficiency (pkt/J)		
	MMCR	m-OLSR	m-OEDR
32	23.9	22.5	17.5
48	13.4	14.5	11.4
60	7.8	9.3	4.9
72	5.7	5.5	3.9
82	7	5.5	4

Table 8. Network overhead for varying node density

Node density	Network Overhead (kbps/node)		
	MMCR	m-OLSR	m-OEDR
32	0.86	0.73	1.6
48	1.5	1.1	2.7
60	1.9	1.45	3.8
72	2.1	1.8	4.1
82	2.5	2.1	5.4

MMCR outperforms the other protocols for higher node densities. On average, MMCR increases throughput by 4.5% over m-m-OLSR, and 30.7% over the m-m-OEDR while it ensures lower end-to-end delay. On an average, MMCR experiences end-to-end delay lesser by 9.2% when compared with m-OLSR and lesser by 40% when compared with m-OEDR. The MMCR is also better in energy efficiency by 2.6% and 41% as compared to m-OLSR and m-OEDR respectively. At high node densities, the congestion levels are higher due to more number of flows. MMCR is able to choose more optimal paths than m-OLSR and m-OEDR to improve the throughput and end-to-end delay performance.

Table 8 shows the network overhead which consistently increases as the number of nodes in the network increase. With an increase in network size, more MPR nodes are needed and selected for routing which in turn generates more HELLO and TC packets. However, the received throughput improves as the number of nodes increase from 32 to 48, even though the number of flows increasing. This is partly due to the fact that with increased network size, the protocols have more choices available for identifying better

routes in order to improve the performance. At the same time, with higher node density, the number of flows and the network overhead also increase causing high congestion levels. As a consequence, the dropped packets increase causing a drop in throughput as observed from Figures 13 and 14. The end-to-end delays also increase as shown in Figure 15.

V. CONCLUSIONS

The proposed MMCR protocol selects paths that provides a tradeoff among throughput, end to end delay, and energy efficiency. MMCR performs better than the m-OLSR and m-OEDR in terms of received throughput, end-to-end delay and energy efficiency for static and mobile network topologies with mobility less than 12 m/s. The m-OLSR chooses the minimum number of hops for routing that often provide suboptimal path since it can select congested nodes to be MPRs. MMCR, on the other hand, chooses MPRs based on the bandwidth factor, energy utilization factor and delay. Thus, MMCR chooses nodes experiencing less or no congestion as MPRs. By contrast, m-OEDR considers only energy and delay in MPR selection and routing and thereby degraded performance. MMCR with higher number of parameters performs better and shows that multiple factors being considered as QoS parameters will improve the performance of the routing protocol even though the network overhead may be increased.

MMCR ensures that the bandwidth factor is greater than one thus causing some flows to be dropped when the network congestion do not allow the desired QoS. Consequently, the bandwidth factor serves as an implicit admission control mechanism which ensures that the flows which are allowed will have better throughput and end-to-end delay.

REFERENCES

[1] P. Gupta and R. Kumar, "The Capacity of Wireless Networks," *IEEE Transactions on Information Theory*, IT-46(2): pp. 388-404, Mar. 2000.

[2] K. Jain, J. Padhye, V. N. Padmanabhan and L. Qiu, "Impact of interference on multi-hop wireless network performance," *MobiCom*, 2003, Vol. 11, no. 4, pp 471-487, July 2005.

[3] "IEEE 802.11b Standard"; standards.ieee.org/getieee802/download/802.11b-1999.pdf

[4] "IEEE 802.11a Standard"; standards.ieee.org/ getieee802/download/802.11a-1999.pdf

[5] "IEEE 802.15.4 Standard";standards.ieee.org/getieee802/download/802.15.4-2006.pdf

[6] Ashish Raniwala, Kartik Gopalan and Tzi-cker Chiueh, "Centralized channel assignment and routing algorithms for multi-channel wireless mesh networks," *Mobile Computing and Communications Review*, vol. 8, no. 2, pp. 50–65, April 2004.

[7] Y. Huang and M. Molle; "An improved topology discovery algorithm for networks with wormhole routing and directed link"; *IEEE Computer Communications and Networks*, pp. 98-105, Sep 1997.

[8] R.Chandra, C. Fetzer and K. Hogstedt; "Adaptive Topology Discovery in Hybrid Wireless Networks"; *Proceedings of Informatics 1st International Conference on Ad Hoc Networks and Wireless*, vol. 16, pp. 1–16, September 2002.

[9] K. C. Claffy, H. W. Braun and G. C. Polyzos; "A parameterizable methodology for Internet traffic flow profiling"; *IEEE JSAC, Journal of Selected Areas in Communications,* vol. 3, issue. 8, pp. 181-1494, October 1995.

[10] Y. J. Lin and M. C. Chan; "A Scalable monitoring approach based on aggregation and refinement"; *IEEE JSAC, Journal of Selected Areas in Communications,* vol. 20, issue. 4, pp. 677-690, May 2002.

[11] M. Alicherry, R. Bhatia and L. Li, "Joint channel assignment and routing for throughput optimization in multi-radio wireless mesh networks," *Proceedings of the 11th annual international conference on Mobile computing and networking, MobiCom'05*, pp. 58-72, September, 2005.

[12] P. Kyasanur and N. Vaidya, "Capacity of multi-channel wireless networks: Impact of number of channels and interfaces," *Proceedings of the 11th annual international conference on Mobile computing and networking, MobiCom'05*, pp. 43-57, August 2005.

[13] R. Draves, J. Padhye and B. Zill, "Routing in multi-radio, multi-hop wireless mesh networks," *Proceedings of the 10th annual international conference on Mobile computing and networking, MobiCom'04*, pp. 114-128, September 2004.

[14] J. So and N. H. Vaidya, "A routing protocol for utilizing multiple channels in multi-hop wireless networks with a single transceiver," *Technical. Report*, University of Illinois at Urbana-Champaign, October 2004.

[15] J. Tang, G. Xue and W. Zhang, "Maximum throughput and fair bandwidth allocation in multi-channel wireless mesh networks," *Proc. of the IEEE INFOCOM*, pp. 1-10, April 2006.

[16] A. Qayyum, L. Viennot and A. Laouiti, "Multipoint relaying for flooding broadcast messages in mobile wireless networks", *Proc. of the 35th Annual Hawaii International Conference on System Sciences, HICSS*, pp. 3866 – 3875, January 2002.

[17] P. Jacquet, P. Muhlethaler, T. Clausen, A. Laouiti, A. Qayyum and L. Viennot, "Optimized link state routing protocol for ad hoc networks", *Proc. of the IEEE International Multi Topic Conference on Technology for the 21st Century, IEEE INMIC'01,* pp. 62 – 68, December 2001.

[18] T. Clausen and P. Jacquet, "Optimized Link State Routing Protocol", *IETF MANET Working Group, Internet Draft,* draft-ietf-manet-olsr-11.txt, July 2003.

[19] N. Regatte and S. Jagannathan "Optimized Energy-Delay Routing in Ad Hoc Wireless Networks," *Proc. of the World Wireless Congress*, May 2005.

[20] P. Bahl, R. Chandra and J. Dunagan, "SSCH: Slotted Seeded Channel Hopping for Capacity Improvement in IEEE 802.11 Wireless Networks," *Proc. of the ACM MobiCom*, pp. 216-230, September 2004.

[21] N. Schacham and P. King, "Architectires and Performance of Multi-channel multi-hop Packet Radio Networks," *IEEE Journal on Selected Area in Communications*, Vol. 5, no. 6, pp. 1013-1025, July, 1987.

[22] A. Adya, P. Bahl, J. Padhye, Alec Wolman and Lidong Zhou, "A multi-radio unification protocol for ieee 802.11 wireless networks," *Proc. of the IEEE International Conference on Broadband Network (Broadnets),* pp. 344-354, 2004.

[23] D. Bertsekas and R. Gallger, *Data Networks*, New Jersey: Prentice Hall, Inc., 1987, pp. 374-380.

[24] R. A. Calvo and J. P. Campo, "Adding Multiple Interface Support in Ns2," http://personales.unican.es/aguerocr/ , May 2008.

[25] NS2 Notebook: Multi-channel Multi-interface Simulation in NS2 (2.29), http://www.cse.msu.edu/~wangbo1/ns2/nshowto8.html

[26] U. Lee and S. F. Midkiff, "OLSR-MC: A Proactive Routing Protocol for Multi-Channel Wireless Ad-Hoc Networks," *Proc. of the IEEE Wireless Communications and Networking Conference, (WCNC 2006),* vol. 1, pp. 331-336, September, 2006.

CONCLUSIONS

In the first paper, a simple diagnostic methodology for determining the product quality measured in terms of the fastener grip length for fastening operations is presented. The feature extraction-based methodology detects normal, over, and under grip cases during the fastening process by employing simple rules; hence it is practical to implement as a real-time decision-making tool.

The hardware implementation and results show that such simple diagnostic methodology is feasible for in-process monitoring of the hand held tools in a network-enabled manufacturing environment. Real-time monitoring of the manufacturing processes and verification of its product quality remove the need for post-process inspection which may be time consuming and cost ineffective. Wireless implementation also shows that such a methodology is practical and reliable for in-process quality monitoring in a shop floor environment.

Such hand-held tools are mobile resources; any type of extended wiring or bulky attachments can interfere with the fastening process. They need to be equipped with relatively small sensors, processing and communication devices so that the proposed approach can be seamlessly implemented. Wireless implementation also enables the remote monitoring of the processes as well as 100% data collection, for future analysis, on each fastener as opposed to traditional statistical process control techniques, which rely on sampling. Similar methodologies implemented over wireless sensor networks can be very effective in other network-enabled manufacturing environments as well.

Overall, the proposed architecture in the first paper has merits to (1) detect and report quality problems in real-time during the process, (2) implement without

complexity by extracting useful features from process signatures and performing simple rule based methodology, and (3) reduce post-process inspection, thereby improving quality while reducing cost and man power. The wireless implementation using single channel wireless networks severely limits the number of tools and their mobility for real-time monitoring and data collection.

Therefore in the second chapter, a multi-interface multi-channel routing protocol (MMCR) is presented which emphasizes on throughput maximization, energy efficiency of the nodes and minimizing end to end delay. Such a protocol will be highly efficient in network enabled manufacturing environments for real-time process monitoring with higher number of mobile hand held tools. Compared to single channel wireless networks, multiple non-interfering channels, when used, improved the amount of data traffic that can be handled in the network lowering congestion while maintaining end-to-end delay and energy efficiency. Multiple channel-based wireless networks offer far greater capacity than the single channel wireless networks. Even in multiple channel routing protocols, consideration of a single parameter for link costs to determine a route are not efficient in achieve optimal performance with respect to QoS parameters of throughput and end to end delay. The proposed routing protocol considers throughput maximization, minimizing end to end delay and improving energy utilization for determining the route which has been verified with the presented results compared to m-OLSR and m-OEDR.

FUTURE WORK

The diagnostic methodology presented in the first paper is a simple rule-based. Such methodologies may not be effective for higher number of data inputs or failure modes as in a multi-actuator pneumatic system. Hence, with the same wireless implementation strategy, statistically and multi-variate based analyses such as Mahalanobis-Taguchi Strategy may be investigated for such complex scenarios.

The multi-channel routing protocol presented in the second paper may be verified and analyzed for real-time applications such as for voice communications through hardware implementation. The routing protocol may also be improved by considering bandwidth allocation among different possible routes. The bandwidth factor used as part of the routing metric may be improvised through channel modeling for including the channel uncertainties and interferences. The routing protocol may be further modified and studied with a dynamic channel assignment algorithm combined with routing.

APPENDIX

For n channel links available between nodes i and j, minimize the cost function $\sum_{i,j} C_{ij}(X_{ij})$, where,

$$Xij = \sum_{p=1}^{n} x_p \tag{1}$$

$\sum_{p=1}^{n} x_p = r$, r – total flow between the nodes (2)

The optimal solution is achieved when the following condition is satisfied:

$$\sum_{p=1}^{n} \frac{\partial C(x^*)}{\partial x_p}(x_p - x_p^*) \geq 0 \tag{3}$$

where, x_p^* is the optimal solution, $x^* = \{ x_p^* \}$

Equation (3) is possible when for all p' element of [0,n]:

$$\frac{\partial C(x^*)}{\partial x_{p'}} \geq \frac{\partial C(x^*)}{\partial x_p} \tag{4}$$

For n channels between two nodes, the cost function is:

$$C(x) = C(x_1) + C(x_2) + \ldots + C(x_n) \tag{5}$$

$$C_i(x_i) = \frac{B_i}{B_i - x_i} \tag{6}$$

B_i is the available bandwidth in channel i.

Therefore, we have:

$$\frac{dC_i}{dx_i} = \frac{B_i}{(B_i - x_i)^2} \tag{7}$$

Case 1: two channels are available, n=2

So, we have,

$$x_1^* + x_2^* = r \tag{8}$$

Assuming, $B_1 > B_2$, we start by assigning the flow completely to channel 1, so that, $x_1 = r$ and $x_2 = 0$.

For equation (4) to satisfy, we have:

$$\frac{dC_1(r)}{dx_1} \leq \frac{dC_2(0)}{dx_2} \tag{9}$$

Using (7) we get:

$$\frac{B_1}{(B_1 - r)^2} \leq \frac{1}{B_2} \tag{10}$$

Case 2: 3 channels are available, n = 3:

We start with, $x_1 = r$, $x_2 = 0$, $x_3 = 0$

Then to satisfy 4,

$$\frac{dC_1(x_1^* = r)}{dx_1} \leq \frac{dC_2(0)}{dx_2}, \text{ and}$$

$$\frac{dC_1(x_1^* = r)}{dx_1} \leq \frac{dC_3(0)}{dx_2} \tag{11}$$

Since, $B_2 > B_3$, and using (7)

$$\frac{B_1}{(B_1 - r)^2} \leq \frac{1}{B_2} \tag{12}$$

Thus, when 2 channels are used irrespective of the number of channels available we get the same condition as in (9) and (12).

Consider , $x_1 = x_1^*$, $x_2^* = r - x_1^*$, $x_3^* = 0$

$$\frac{dC(x^*)}{dx_1} = \frac{dC_1(x_1^*)}{dx_1} + \frac{dC_2(x_2^*)}{dx_2} + \frac{dC_3(x_3^*)}{dx_3}$$

$$\frac{dC(x^*)}{dx_1} = \frac{B_1}{(B_1 - x_1^*)^2} - \frac{B_2}{(B_2 - r + x_1^*)^2} + 0 \tag{13}$$

Similarly,

$$\frac{dC(x^*)}{dx_2} = \frac{-B_1}{(B_1 - r + x_2^*)^2} + \frac{B_2}{(B_2 - x_2^*)^2} + 0 \tag{14}$$

$$\frac{dC(x^*)}{dx_3} = 0 + 0 + \frac{1}{B_3} \tag{15}$$

For equation (4) to satisfy:

$$\frac{dC(x^*)}{dx_1^*} \leq \frac{dC(x^*)}{dx_2} \tag{16}$$

$$\frac{dC(x^*)}{dx_1^*} \leq \frac{dC(x^*)}{dx_3} \tag{17}$$

and,

$$\frac{dC(x^*)}{dx_2^*} \leq \frac{dC(x^*)}{dx_1} \tag{18}$$

$$\frac{dC(x^*)}{dx_2^*} \leq \frac{dC(x^*)}{dx_3} \tag{19}$$

(16) and (18) are satisfied as the expressions on the L.H.S. and R.H.S. are equal.

From (13), (15) and (17), we have:

$$\frac{B_1}{(B_1 - x_1^*)^2} - \frac{B_2}{(B_2 - r + x_1^*)^2} \leq \frac{1}{B_3} \tag{20}$$

$$\frac{B_2}{(B_2 - x_2^*)^2} - \frac{B_1}{(B_1 - r + x_2^*)^2} \leq \frac{1}{B_3} \tag{21}$$

Generalizing (20) and (21) for n channels and x_j must satisfy:

$$\frac{B_j}{(B_j - x_j)^2} - \sum_{\substack{i=1 \\ i \neq j}}^{k-1} \frac{Bi}{(Bi - r + \sum_{\substack{m=1 \\ m \neq i}}^{k-1} x_i)^2} \leq \frac{1}{B_k} \tag{22}$$

VITA

Reghu Anguswamy was born in Trivandrum, Kerala, India on January 9, 1983. He completed his Bachelor of Technology degree in Electronics and Communication from College of Engineering – Trivandrum (University of Kerala) in May 2004. He joined University of Missouri-Rolla in Spring 2006 for a Master of Science program in Systems Engineering and received the degree in December 2008.